REPORT DOCUMENTATION PAGE

The public reporting burden for this collection of information is estimated to average 1 hour per response, including the time for reviewing instructions, searching existing data sources, gathering and maintaining the data needed, and completing and reviewing the collection of information. Send comments regarding this burden estimate or any other aspect of this collection of information, including suggestions for reducing the burden, to Department of Defense, Washington Headquarters Services, Directorate for Information Operations and Reports (0704-0188), 1215 Jefferson Davis Highway, Suite 1204, Arlington, VA 22202-4302. Respondents should be aware that notwithstanding any other provision of law, no person shall be subject to any penalty for failing to comply with a collection of information if it does not display a currently valid OMB control number. **PLEASE DO NOT RETURN YOUR FORM TO THE ABOVE ADDRESS.**

1. REPORT DATE (DD-MM-YYYY)	2. REPORT TYPE	3. DATES COVERED (From - To)
07/24/2012	Interim Research Performance Report	5/1/2012 - 7/31/2012

4. TITLE AND SUBTITLE
Interim Research Performance Report
Quarterly Report No. 4

5a. CONTRACT NUMBER

5b. GRANT NUMBER
N00014-11-1-0752

5c. PROGRAM ELEMENT NUMBER

6. AUTHOR(S)
Murray, Nathan E.

5d. PROJECT NUMBER

5e. TASK NUMBER

5f. WORK UNIT NUMBER

7. PERFORMING ORGANIZATION NAME(S) AND ADDRESS(ES)
The University of Mississippi
Jamie Whitten National Center for Physical Acoustics
University, MS 38677

8. PERFORMING ORGANIZATION REPORT NUMBER

9. SPONSORING/MONITORING AGENCY NAME(S) AND ADDRESS(ES)
Joseph Doychak
Office of Naval Research
875 North Randolph Street
Arlington, VA 22203-1995

10. SPONSOR/MONITOR'S ACRONYM(S)
ONR

11. SPONSOR/MONITOR'S REPORT NUMBER(S)

12. DISTRIBUTION/AVAILABILITY STATEMENT
Approved for Public Release; Distribution is Unlimited

13. SUPPLEMENTARY NOTES
In collaboration with Charles Tinney (U. of Texas at Austin), Brian Thurow (Auburn Univ.), & Raj Sinha (CRAFT Tech)

14. ABSTRACT
Progress was made on the analysis methodology for the HDR-PIV. Characteristic results describing the general nature of the acoustics for the measured jets was compiled and accepted for publication in the ASME INTERNOISE 2012 conference. A brief overview of the entire Year 1 effort was presented at the AFOSR/ONR Joint Aerothermodynamics Review.

15. SUBJECT TERMS
Jet Noise Reduction

16. SECURITY CLASSIFICATION OF:			17. LIMITATION OF ABSTRACT	18. NUMBER OF PAGES	19a. NAME OF RESPONSIBLE PERSON
a. REPORT	b. ABSTRACT	c. THIS PAGE			Nathan E. Murray
				37	19b. TELEPHONE NUMBER (Include area code) 662-915-3190

Quarterly Progress Report No. 4

1 MAY 2012 – 31 JULY 2012

Nathan E. Murray (PI)
Aeroacoustics Research Group
National Center for Physical Acoustics
University of Mississippi
University, MS 38677
(662) 915-3190
nmurray@olemiss.edu

Contract: N00014-11-1-0752

Contract Monitor: Joseph Doychak
Office of Naval Research
Arlington, VA 22203-1995
joseph_doychak@onr.mil

Executive Summary

Progress was made on the analysis methodology for the HDR-PIV. Characteristic results describing the general nature of the acoustics for the measured jets was compiled and accepted for publication in the ASME INTERNOISE 2012 conference. A brief overview of the entire Year 1 effort was presented at the AFOSR/ONR Joint Aerothermodynamics Review.

20120730055

July 24, 2012

1 Project Objectives and Status

The presentation of the Year 1 accomplishments offered an opportunity for reflection on the objectives of the program. Indeed, the main technical objective of Year 1, the joint experimental effort between all the institutions, was successfully conducted. However, it is also evident that the focus on resolving the technical hurdles presented by the experiment itself has distracted from maintaining clarity in the overall purpose. For example, given that the MHz rate PIV were able to generate all the data that was anticipated, what scientific purpose will the data be used to fulfill?

As Year 2 begins, a concerted effort will be made to clarify the purpose of the experimental activities beyond simply producing archival data.

1.1 Project Status

An updated project chart is shown in Figure 1 which details the WBS items from the SOW and the completion percentages as of the end of the reporting period.

2 Activity for Current Reporting Period

Progress has been made on the analysis of the HDR-PIV data. It seems promising that an increased signal-to-noise ratio may be possible, but the full benefits of the data set have yet to be exercised. Characteristic results were presented in the Year 1 review meeting.

Additional acoustic data was collected in July using PCB microphones in the near-field as a comparative check on the Kulite data acquired in February and April of 2012. This July data set also included sweeps of temperature range and pressure ratio that may be of interest to the community for benchmark purposes.

Preliminary research into the use of information entropy to assess near-field to far-field propagation has been conducted. The concept is a statistical measure known to the digital communication world that provides a measure of the mutual information between two streams of data. The initial impression is that this measure may prove useful in defining a relevant cost function that is measurable in the near field for active control purposes.

3 Technical/Cost Status & Problem Areas

The April experimental effort to acquired MHz rate PIV demonstrated the shortfalls of the current seeding system. Through a separate NAVAIR funded effort, a new pH balanced, liquid based, seeder system is being built for use in Year 2 experiments. The new seeder is being patterned after that developed by Mark Wernet at NASA Glenn for hot supersonic flows.

4 Publications, Meetings, and/or Travel

A conference paper titled, "A Laboratory Framework for Synchronous Near/Far-Field Acoustics and MHz PIV in High-Temperature, Shock-Containing, Jets," was submitted and ac-
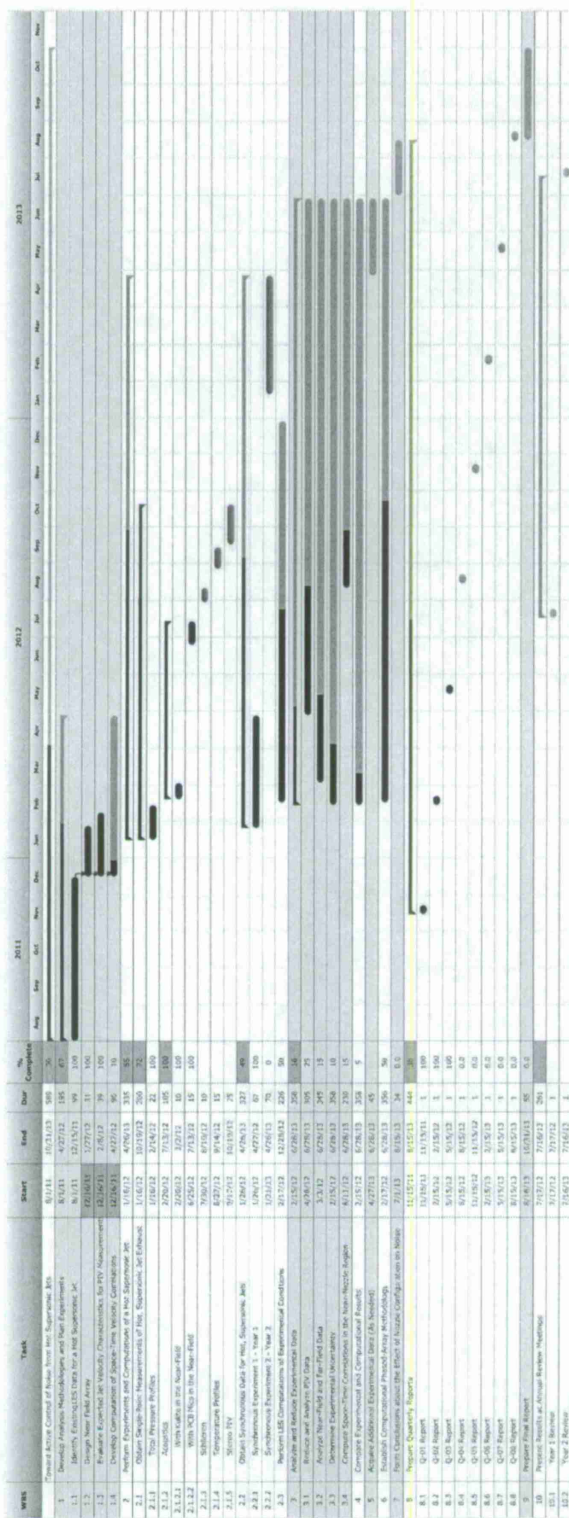
Figure 1. Project chart showing WBS items and current completion status as of the end of the reporting period.

cepted for presentation at the ASME INTERNOISE 2012 conference to be held in August. A copy of the paper is included here as Appendix B.

Drs. Murray and Tinney traveled to U. of Florida, Research Engineering and Education Facility to present the Year 1 review at the 2012 AFOSR/ONR Joint Aerothermodynamic Review held on 17 July. The presentation is included here as Appendix A.

5   Planned Activities for Next Reporting Period

- Critically access the goals of the experimental effort.

- Conduct remaining data collection to complete the description of the jet characteristics.

- Present paper at the ASME/NCAD INTERNOISE 2012 conference.

Appendix A: Year 1 Review Presentation Given at the 2012 AFOSR/ONR Joint Aerothermodynamics Review

Toward Active Control of Noise from Hot Supersonic Jets

2012 AFOSR/ONR Joint Aerothermodynamics Review

Prepared By:
Nathan E. Murray
National Center for Physical Acoustics (NCPA)
University of Mississippi
University, MS 38677
(662) 915-3190
nmurray@olemiss.edu

17 July 2012

THE UNIVERSITY OF MISSISSIPPI

NATIONAL CENTER FOR PHYSICAL ACOUSTICS

2012 AFOSR/ONR Joint Aerothermodynamics Review   Page 2

OUTLINE

▷ Objectives

▷ Year 1 Accomplishments

▷ Nozzle Configurations and Characteristic Results

  – N. Murray, U. Miss. NCPA

  – CRAFT Tech CFD, P. Panickar, N. Sinha

▷ Preliminary HDR-PIV Results

  – B. Thurow, U. Auburn

▷ Predicting the Formation of Cumulative Non-Linearities

  – C. Tinney, U. T. Austin

▷ Plans for Year 2

THE UNIVERSITY OF MISSISSIPPI

NATIONAL CENTER FOR PHYSICAL ACOUSTICS

Page 3

OBJECTIVES

▷ Exp. Characterization of Hot, Shock-Containing, Supersonic Jets

  – Time-resolved characterization of the development of large-scale structures,
  – Synchronous pressure measurements in the hydrodynamic periphery,
  – Simultaneous far-field acoustic measurements.

▷ Quantify Linear and Non-Linear Coherence/Propagation

▷ Advance Computational Modeling and Noise Source Localization

THE UNIVERSITY OF MISSISSIPPI
NATIONAL CENTER FOR PHYSICAL ACOUSTICS

Page 4

YEAR 1 ACCOMPLISHMENTS

THE UNIVERSITY OF MISSISSIPPI
NATIONAL CENTER FOR PHYSICAL ACOUSTICS
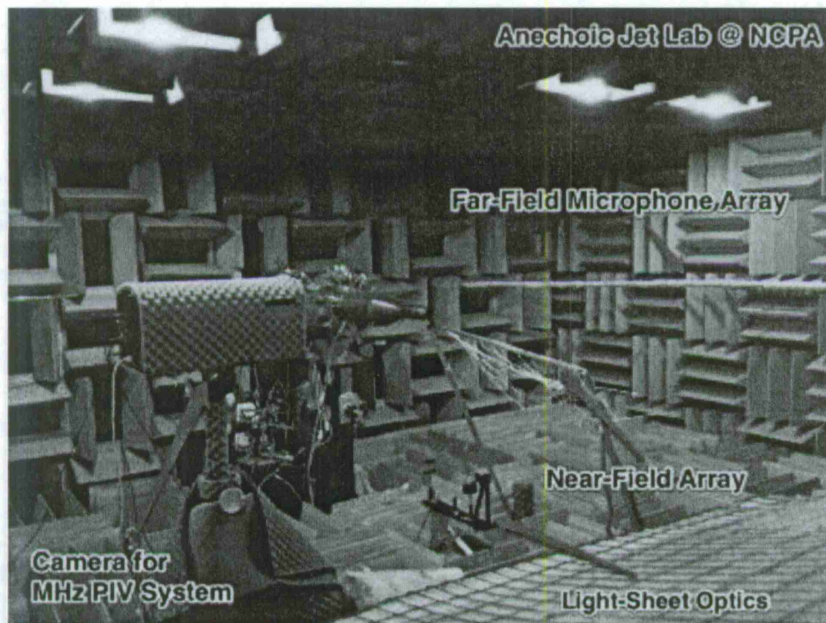
YEAR 1 ACCOMPLISHMENTS

▷ Largely Student Led Effort

- 1 Graduate Student from Each Institution
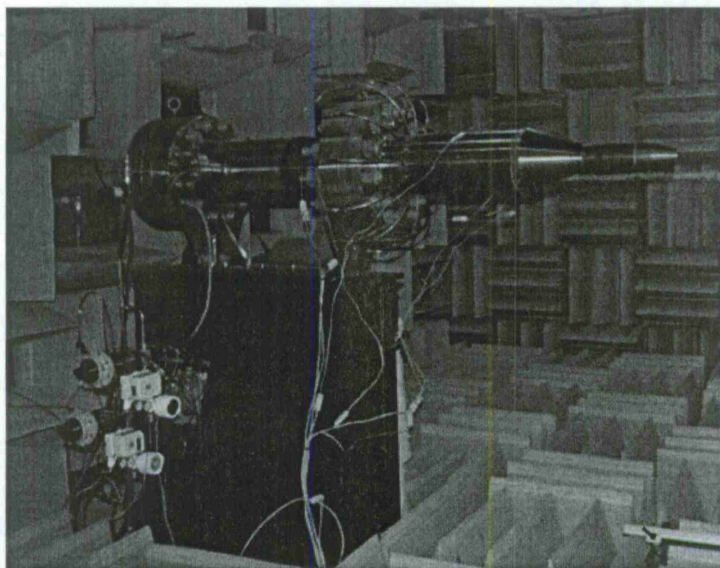- Students in Residence at U. Miss. for duration of the joint experimental effort.
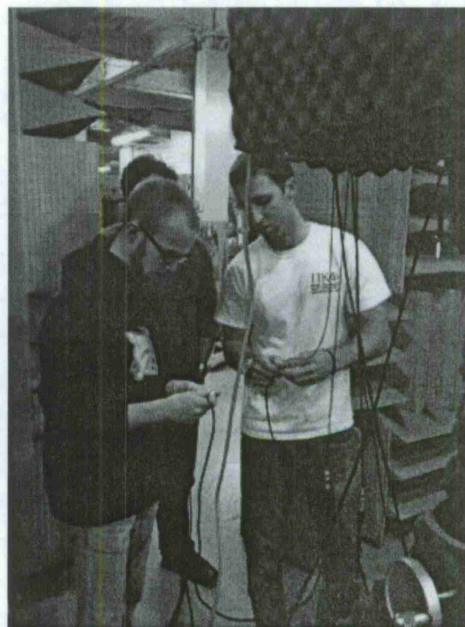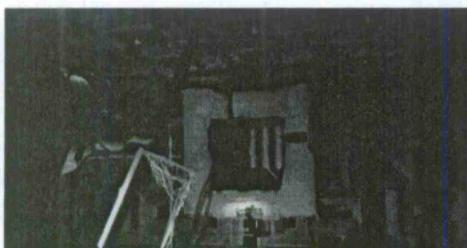
THE UNIVERSITY OF MISSISSIPPI
NATIONAL CENTER FOR PHYSICAL ACOUSTICS

NOZZLE CONFIGURATIONS
NCPA ANECHOIC JET LABORATORY

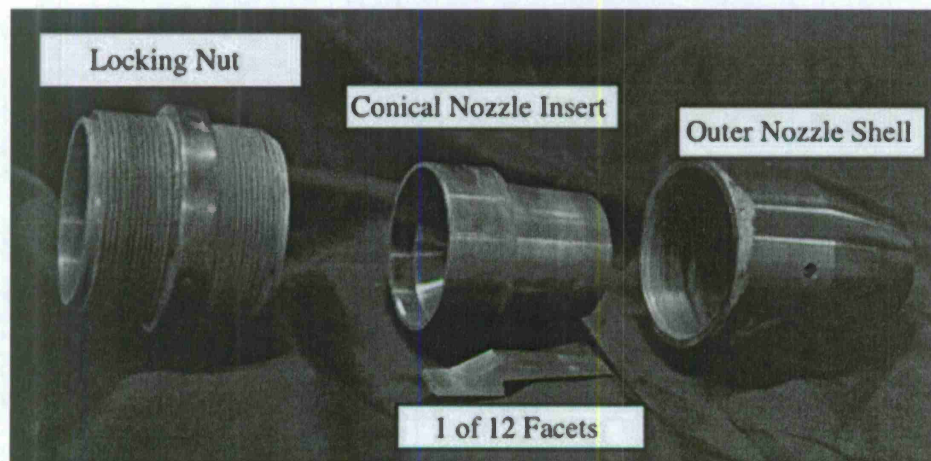THE UNIVERSITY OF MISSISSIPPI
NATIONAL CENTER FOR PHYSICAL ACOUSTICS

NOZZLE CONFIGURATIONS

'MILITARY STYLE' NOZZLE MODEL

Locking Nut

Conical Nozzle Insert

Outer Nozzle Shell
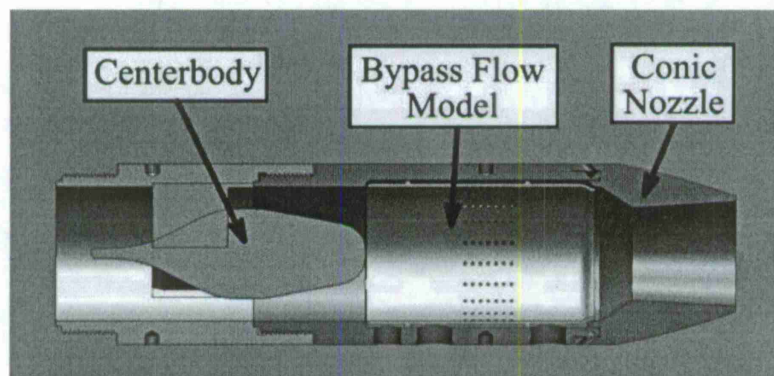
1 of 12 Facets

▷ Modular Nozzle System

▷ All Inconel Construction

THE UNIVERSITY OF MISSISSIPPI

NATIONAL CENTER FOR PHYSICAL ACOUSTICS

NOZZLE CONFIGURATIONS

'MILITARY STYLE' NOZZLE MODEL

Centerbody

Bypass Flow Model

Conic Nozzle

▷ Nozzle Configurations Being Utilized:

– Conic Nozzle without Centerbody

– Conic Nozzle with Centerbody

– Faceted Nozzle without Centerbody

THE UNIVERSITY OF MISSISSIPPI

NATIONAL CENTER FOR PHYSICAL ACOUSTICS

NOZZLE CONFIGURATIONS

FOR NCPA ANECHOIC JET LABORATORY

▷ Nozzle Conditions Being Examined

- Geometrical
  - $A/A^\star \rightarrow M_d = 1.74$
- Acoustic Data Collected: Conic & Conic w/ Centerbody
  - T_0/T_∞ from $2.3 \rightarrow 3.4$ at $NPR = 5.2$ and 3.9
  - NPR from $4.0 \rightarrow 6.0$ at $T_0/T_\infty = 3.0$
  - Feb 2012 (limited range of conditions) & July 2012
- Joint Acoustic, HDR-PIV Data Collected: Conic w/ Centerbody
  - $T_0/T_\infty = 3.35$ and $NPR = 3.96$
  - April 2012
- CFD Computations Being Conducted: Conic & Conic w/ Centerbody
  - $T_0/T_\infty = 3.35$ and $NPR = 3.96$
  - $T_0/T_\infty = 3.35$ and $NPR = 5.24$
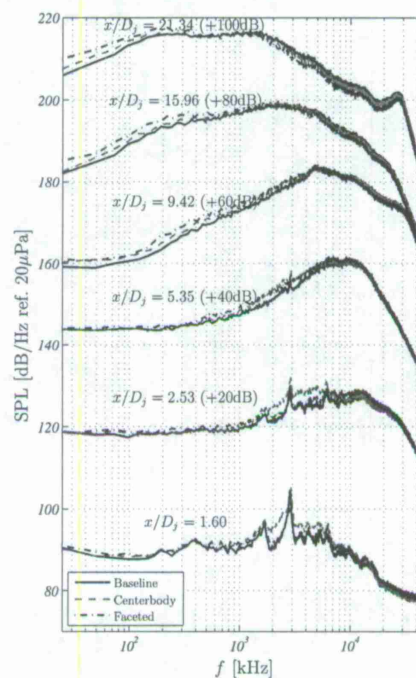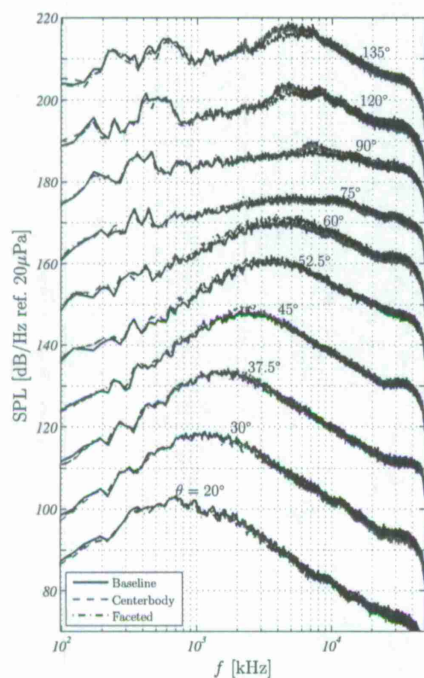 - Ongoing Using Hybrid RANS/LES Implementation in CRAFT®
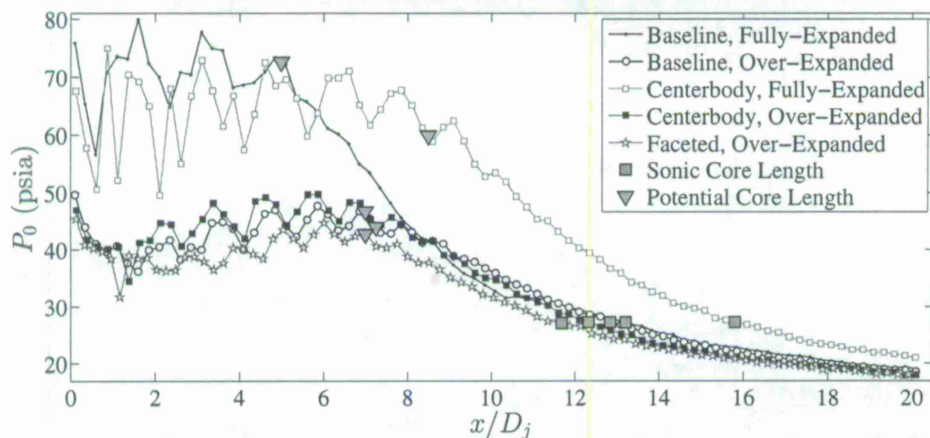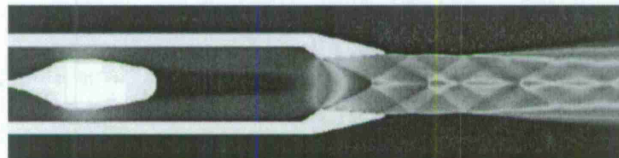
THE UNIVERSITY OF MISSISSIPPI
NATIONAL CENTER FOR PHYSICAL ACOUSTICS

GENERAL CHARACTERISTICS

THE UNIVERSITY OF MISSISSIPPI
NATIONAL CENTER FOR PHYSICAL ACOUSTICS

GENERAL CHARACTERISTICS

DISCUSSION OF RESULTS TO DATE

▷ Preliminary HDR-PIV Results

▷ Predicting the Formation of Cumulative Non-Linearities

THE UNIVERSITY OF MISSISSIPPI

NATIONAL CENTER FOR PHYSICAL ACOUSTICS

Preliminary Results: High Dynamic Range (HDR) PIV
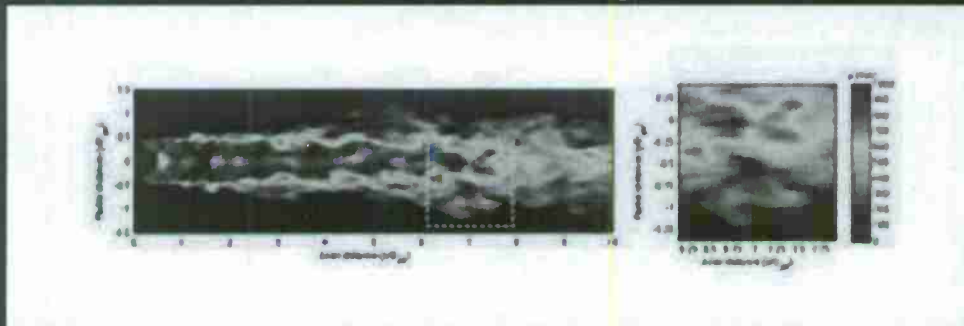
R. Harris Haynes, Dr. Brian S. Thurow

Advanced Laser Diagnostics Laboratory
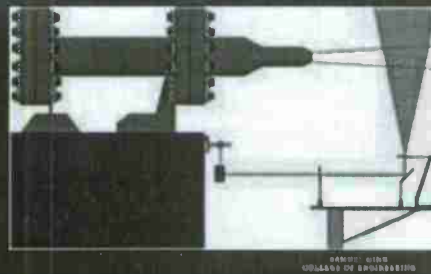Department of Aerospace Engineering

9 July 2012

AUBURN UNIVERSITY
SAMUEL GINN
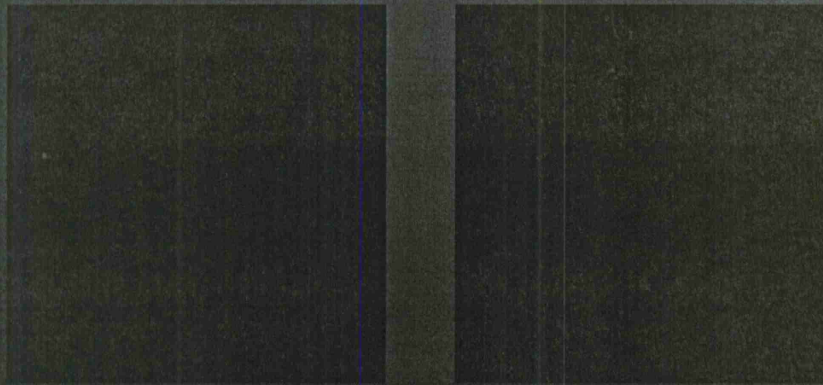COLLEGE OF ENGINEERING

Experimental Arrangement

- The imaged region, enclosed by the dashed lines, was centered axially 7 turret diameters downstream of the nozzle exit and radially along the bottom shear layer of the jet.

Sample Image Sequences

- Each image sequence contains 16 frames acquired at a 1 MHz framing rate. The movies shown represent 2 such sequences, each spanning a temporal window of only 15 μs.

AUBURN UNIVERSITY
SAMUEL GINN
COLLEGE OF ENGINEERING

High Dynamic Range (HDR) PIV
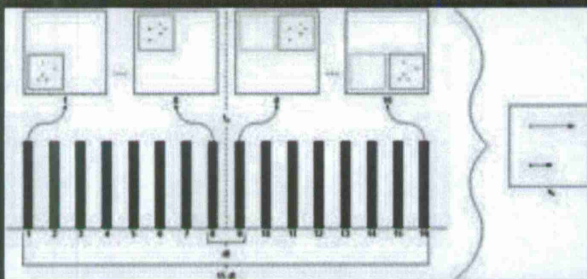
Dynamic velocity range refers to the maximum and minimum resolvable particle displacements.

- This range can be increased by utilizing local velocity measurements from multiple image pairs with varying temporal spacings. Significant improvements over conventional PIV results can be made in this way, especially in flows containing wide velocity ranges.

AUBURN UNIVERSITY
SAMUEL GINN
COLLEGE OF ENGINEERING

Conventional Velocity Fields
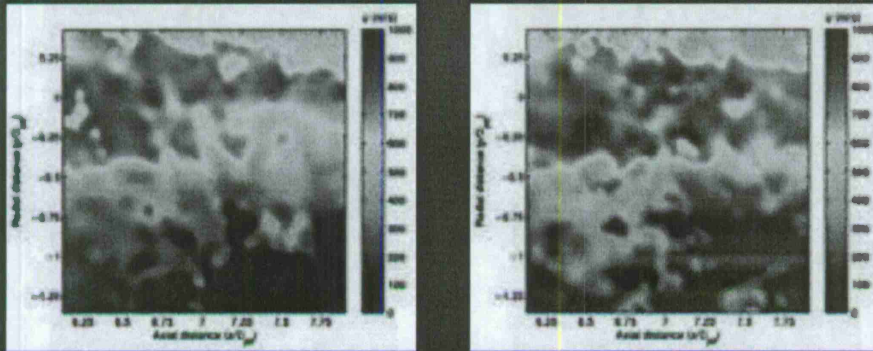
- The contours above are conventional, temporally-resolved PIV results indicating streamwise velocity. The profiles were determined using image pairs 1-2 and 2-3, respectively, and have a temporal spacing of 1 μs.

HDR Velocity Field
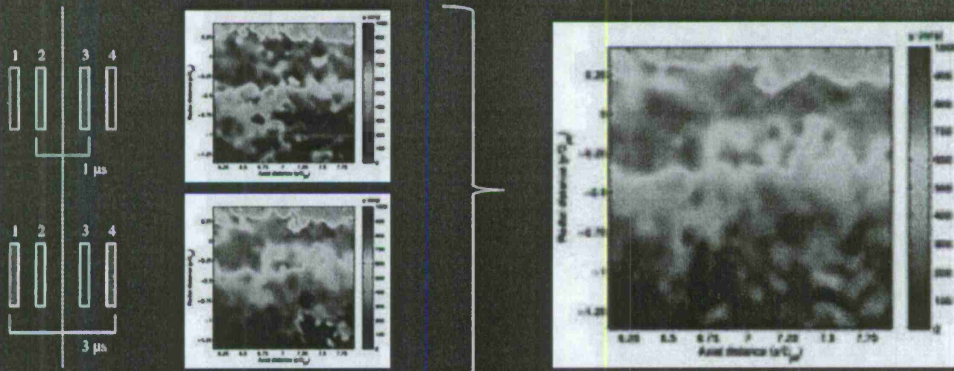
- The plots on the left represent the same conventional PIV velocity field. The plot on the right also shows this field but was compiled using the HDR approach. Velocities selected for the HDR result were based entirely on the SNR.

Error Analysis

- Sequences containing 2 sets of 8 frames each were acquired with no temporal spacings such that any velocity measurements between frames would be directly attributable to experimental error.

- The average or bias error found between any 2 frames is correctable, however the random error limits the maximum attainable accuracy for the velocity measurements.

AUBURN UNIVERSITY

2012 AFOSR-ONR Joint Aerothermodynamics Review

ONR
Office of Naval Research

A model for predicting the formation of cumulative non-linearities from jet flows.

N00014-11-1-0752

New Start: ONR

Woutijn J. Baars, Dr. Charles E. Tinney
The University of Texas at Austin
Department of Aerospace Engineering and Engineering Mechanics
Austin, TX 78712
cetinney@mail.utexas.edu
http://www.ae.utexas.edu/facultysites/tinney/

The University of Texas at Austin   cetinney@mail.utexas.edu   http://www.ae.utexas.edu/facultysites/tinney/

FIGURE 32. (a) Power spectra of the linear and nonlinear predicted time series at $\rho/D_j = 140$ and the power spectra of the input waveform at $\rho/D_j = 60$. (b) Comparison of the predicted and measured spectra at location $\rho/D_j = 140$ (5% bandwidth moving filter applied).

FIGURE 30. (a) The normalized quadrature spectral density along the spreading lines A-G (5% bandwidth moving filter applied).

2012 AFOSR-ONR Joint Aerothermodynamics Review

ONR · Office of Naval Research

- Cumulative waveform distortions require two ingredients:
  (1) High particle velocities in the initial waveform
  (2) Favorable atmospheric absorption losses
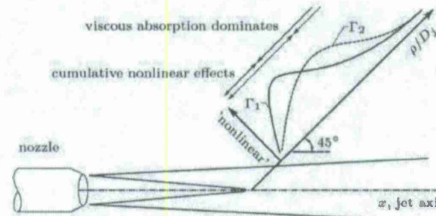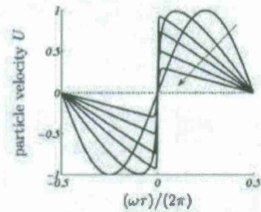
- What conditions are required for this to occur in the far-field of a jet flow?
  - Determine the <u>effective</u> Gol'dberg number:

$$\Gamma = \frac{l_a}{\bar{r}} = \frac{1}{\alpha\bar{r}}$$

- Model assumptions:
  - Progressive broadband Gaussian source!

$$\bar{r} = r_0 \, exp\left(\pm\bar{x}/r_0\right)$$

  - Equal medium (air)
  - Strouhal numbers match for same Mach number and Temperature ratios between laboratory and full scale conditions
  - ? - Source scale needed for spherical propagation equation.
- We employ complete absorption effects:
  - Thermoviscous
  - Molecular relaxation (oxygen and nitrogen)

The University of Texas at Austin   cetinney@mail.utexas.edu   http://www.ae.utexas.edu/facultysites/tinney/

2012 AFOSR-ONR Joint Aerothermodynamics Review

ONR · Office of Naval Research
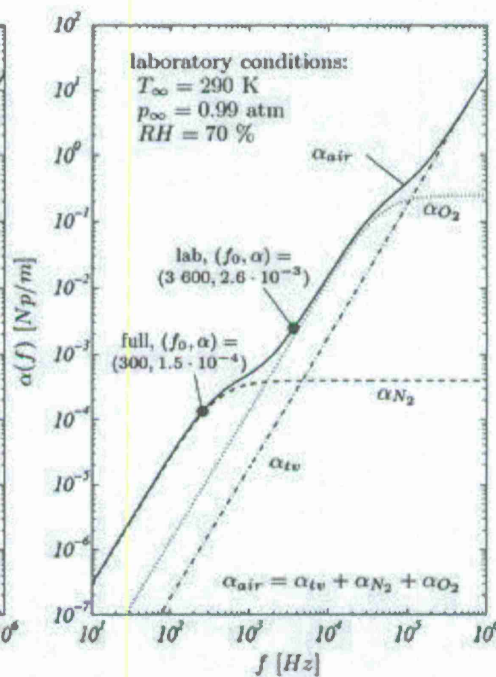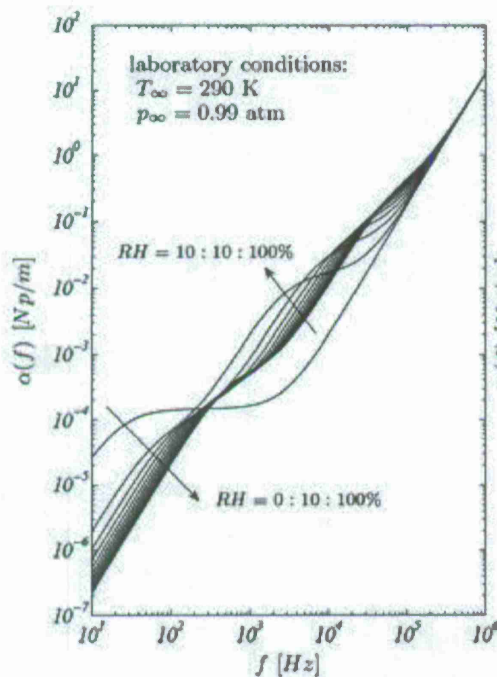
The University of Texas at Austin   cetinney@mail.utexas.edu   http://www.ae.utexas.edu/facultysites/tinney/
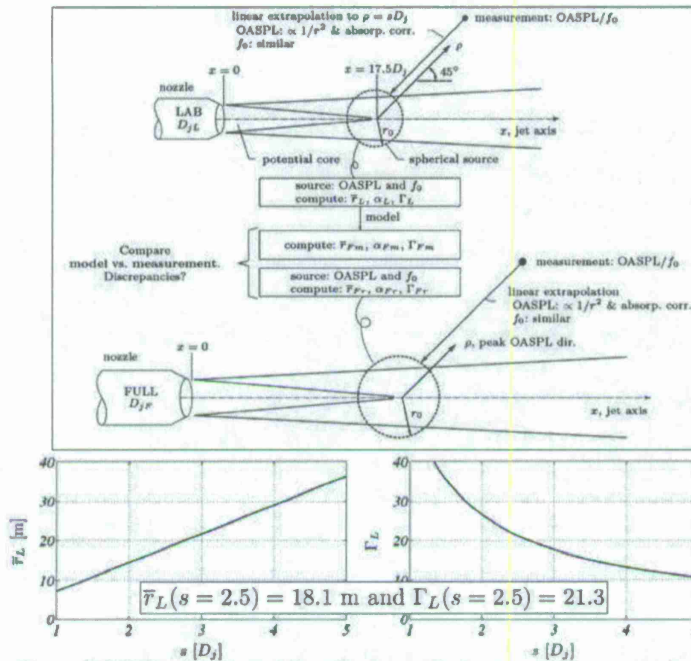
FIGURE 19. (a) The spherical shock formation distance for the current laboratory scenario as function of source size ($r_0 = sD_j$). (b) The effective Gol'dberg number in the laboratory case as function of source size.

- Normalized shock formation distance.
  - Relating laboratory scales (L) to full scales (F) conditions of practical interest.

$$\frac{\overline{r}_L}{D_{jL}} = \left(\frac{\overline{r}_F}{D_{jF}} \right)^{\eta} s^{(1-\eta)}$$

  - Relationship based on common jet exit parameters

$$\eta = \eta \left(M_j, T_j, St_{D_j} \right) = \frac{\overline{x}_L / r_{0L}}{\overline{x}_F / r_{0F}}$$
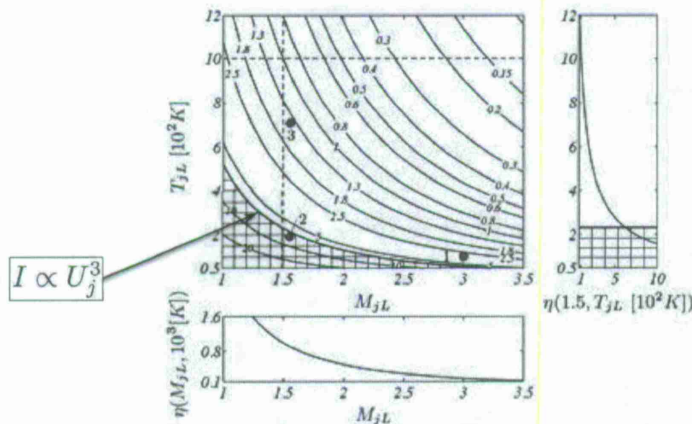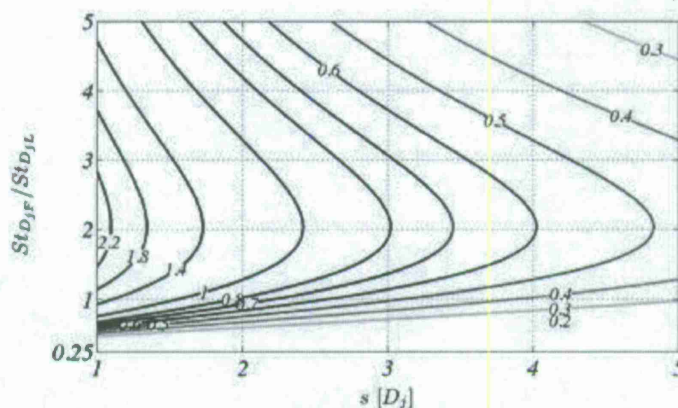
FIGURE 22. The effective Gol'dberg number for the full-scale case as is predicted by the model, $\Gamma_{Fm}(s, St_{D_{jF}})$, (multiply by 1 000).

	l_a [m]	$\overline{x}$ [m]	$\overline{r}$ [m]	$\overline{r}/D_j$	Γ	ΓD_j [m]
Laboratory (measured)	385	0.36	18.1	713	21.3	0.541
Full–scale (model)	6733	2.56	6.98	7.35	965	916
Full–scale (Gee *et al.* 2008)	6733	0.82	3.35	3.53	2010	1910

TABLE 4. Summary of the nonlinear characteristic parameters in the laboratory case and full-scale cases (model and measurement) when the source size is fixed at $s = 2.5$.

We are pretty convinced of the following

- Acoustic waveforms are distorted at birth due to nature of Mach wave radiation process
  - These waveforms have **not** undergone cumulative nonlinear distortion...I know they look like it, but they have not.
- Most, if not all, laboratory scale jets are being studied in range restricted environments.
  - This means that we **cannot** accurately capture cumulative nonlinear distortions in our labs
  - Shock formation distances increase (increased absorption) with decreasing jet diameter
    - It does not scale geometrically with nozzle diameter....equal medium condition
- Full scale studies are required to accurately capture cumulative non-linear distortions produced by Mach wave radiation
  - Has Kent Gee cornered the market on this?
- The Texas code works! (Burgers equation).
 - See Gee's application of this to full scale jets.

- Overhasty conclusions regarding the change in high frequencies in your lab due to non-linear distortion means you have chosen the wrong propagation path.
  - You need to map out the far-field pressure (OASPL)
- Correct propagation path emanates from the post-potential core regions of the flow...not the jet exit plane!

- Crackle is a psycho acoustics problem.
  - Did you listen to the waveform to hear if distortion effects are present?

[1] Baars, W.J., Tinney, C.E., Wochner, M.S. (2012) Nonlinear noise propagation from a fully expanded Mach 3 jet. 50th AIAA Aerospace Sciences Meeting and Exposition, Nashville, U.S.A. Paper 2012-1177.
[2] Baars, W.J., Tinney, C.E., Wochner, M.S. Part 1: Noise propagation from a fully expanded Mach 3 jet: Crackle of nonlinear features? Manuscript in preparation.
[3] Baars, W.J., Tinney, C.E., Part 2: Noise propagation from a fully expanded Mach 3 jet: shock detection. Manuscript in preparation.

Plans for Year 2

▷ Complete CFD Simulations

▷ Implement a pH-Balanced Fluid-Based Seeder System

▷ Address Software & Optics Issues with Camera System

▷ Perform a Second Joint Experiment

▷ Acquire Additional Characteristic Data

  – Schlieren Imaging
  – Standard 3-Component PIV
  – Additional Probe Based Measurements: Total Temperature

▷ Prepare an Archived Data Set

▷ Shift Focus to Data Analysis

The University of Mississippi

National Center for Physical Acoustics

Appendix B: ASME INTERNOISE 2012 Paper 1270 – "A Laboratory Framework for Synchronous Near/Far-Field Acoustics and MHz PIV in High-Temperature, Shock-Containing, Jets"

ASME/NCAD-1270

A LABORATORY FRAMEWORK FOR SYNCHRONOUS NEAR/FAR-FIELD ACOUSTICS AND MHZ PIV IN HIGH-TEMPERATURE, SHOCK-CONTAINING, JETS

N. Murray* & G. Lyons

Jamie Whitten National Center
for Physical Acoustics
The University of Mississippi
University, Mississippi 38677
Email: nmurray@olemiss.edu

C. E. Tinney, B. Donald & W. Baars

Dept. of Aerospace Engineering
and Engineering Mechanics
The University of Texas at Austin
Austin, Texas 78712

B. Thurow & H. Haynes

Advanced Laser Diagnostics Lab
Dept. of Aerospace Engineering
Auburn University
Auburn, Alabama 36849

P. Panickar

Combustion Research and Flow Technology, Inc.
Pipersville, PA 18947

ABSTRACT

This paper describes the experimental study of the noise generating characteristics of high-temperature, shock-containing jets emanating from conic-section, converging-diverging (C-D) nozzles. Conic C-D nozzles consist of two conic sections, one contracting and the other expanding, joined to form a supersonic nozzle with a very sharp radius of curvature at the nozzle throat. An experiment is conducted in which temporally resolved flow-field measurements are acquired simultaneously with near-field and far-field acoustics to allow investigation of the turbulence associated with noise generation. The MHz rate PIV system and its synchronization with acoustic measurements is described along with methods for data analysis. General acoustic results are presented to characterize the spectral content present, and preliminary results on the measured turbulence structures are discussed.

NOMENCLATURE

A_e Nozzle exit area.

A_t Nozzle throat area.

AR   Exit-to-throat area ratio, $AR = A_e/A_t$.

AJL   Anechoic Jet Laboratory.

D_j Nozzle exit diameter.

M_a Acoustic Mach number.

M_d Nozzle design Mach number based on AR.

M_j Jet Mach number computed from the NPR.

U_j Jet exit velocity.

NPR   Nozzle pressure ratio, $NPR = P_0/P_a$.

P_0 Jet stagnation pressure.

P_a Ambient pressure measured inside the AJL.

x Axial coordinate, $x = 0$ at the nozzle exit, positive in the flow direction.

r Radial coordinate such that $r/D_j = 0.5$ at the nozzle lip.

θ Polar angle measured from the positive x-axis.

PBL   Pulse Burst Laser System

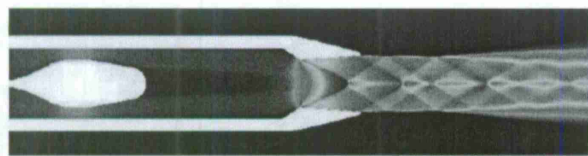*Address all correspondence to this author.

1

FIGURE 1. The mean velocity field (CFD computation) for the Centerbody configuration at fully-expanded conditions illustrating the shock structure in the plume.

INTRODUCTION

Jet noise generated by supersonic flows from converging-diverging nozzles that generate internal shocks possess an added level of complexity in that they include an additional shock system in the jet plume and can involve flow separation inside the diverging section of the nozzle. Typical variable area nozzles found on modern high-performance military aircraft are representative of this situation. A renewed interest in studying the related jet noise has been prompted by the US Navy to specifically address the noise-induced hearing loss and degraded operational awareness resulting from the ever increasing noise levels of higher thrust engines [1, 2].

The present work focuses specifically on the noise generating characteristics of high-temperature, shock-containing jets emanating from conic-section, converging-diverging (C-D) nozzles. A conic C-D nozzle here describes the joining of two conic sections, one contracting and the other expanding, to form a supersonic nozzle with a very sharp radius of curvature at the nozzle throat. The near discontinuity in the slope of the nozzle contour at the throat generates a shock even when the nozzle is operated at its design Mach number, M_d. This is illustrated in Fig. 1 which shows the mean streamwise velocity field computed using a Hybrid RANS/LES approach.

To study the noise generating features of these jets with sufficient temporal fidelity, a synchronized system is here developed that includes a MHz rate PIV system, and near-field pressure transducer array, and a far-field microphone array. The MHz rate flow measurement system offers the opportunity to obtain time-resolved, high-dynamic range velocity measurements. Synchronizing the PIV with the near-field and far-field arrays provides the means for evaluating the noise generation and propagation.This laboratory framework shares similarities to previous recent works utilizing either high-frame-rate PIV [3, 4] and/or near-field/far-field correlation measurements [5–7].

While no results from the fully synchronous system have yet been obtained, the various components and the synchronized data acquisition system are here described in detail. A discussion of the high-dynamic range PIV analysis methodology is presented along with preliminary flow-visualization results obtained with the pulse burst laser system. To characterize the jet itself, the bulk of the paper focuses on the results of mean flow probe
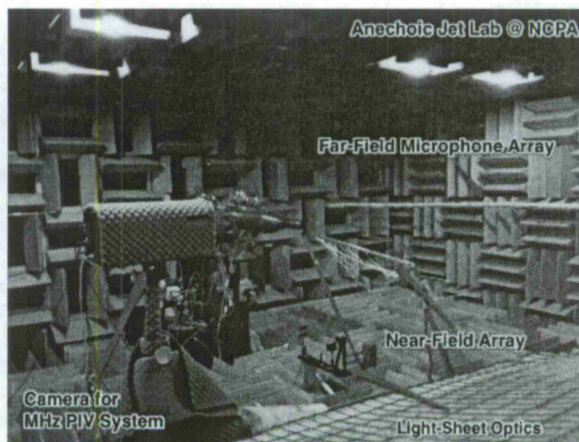
FIGURE 2. The NCPA Anechoic Jet Laboratory setup for the simultaneous near-field/far-field/MHz-PIV measurements.

measurements and the near-field and far-field acoustic data.

DETAILS OF THE EXPERIMENTAL SETUP

To date, three main experimental entries have been completed. The first measured the mean total pressure distribution for each jet configuration. The second measured the fluctuating pressure field using a near-field line array of pressure transducers simultaneously with a far-field arc array of microphones for each jet configuration. The third entry involved the synchronous measurement of the near-field and far-field pressure along with particle image velocimetry (PIV) measurements of the velocity field use a MHz rate system. A description of the experimental facility and setup for each of these components is discussed below.

Anechoic Jet Laboratory

The Anechoic Jet Laboratory (AJL) at the University of Mississippi's National Center for Physical Acoustics is a small facility purpose built for the study of high-temperature, supersonic jet noise [8, 9]. The facility was designed with upstream and downstream "stagnation" chambers through which ambient air is pulled by a 10,000 SCFM fan. The air is allowed to percolate into the 19-by-20-by-8 foot chamber (wedge tip to wedge tip) through 50% porosity sliding panels achieving approximately 1 ft/s in the anechoic section (without jet flow). The openings in the upstream wedge wall allowing the aspiration of the chamber can be seen in Fig. 2. The aspiration of the chamber results in a very even temperature distribution throughout the room and allows the jet entrainment to be less effected by the enclosed space.

The jet rig utilizes a propane burner system as shown in

2 Copyright © 2012 by ASME

FIGURE 3. Illustration of the propane burner system and nozzle assembly.

Fig. 3. Air is supplied from an 1100 hp Ingersoll-Rand Centac compressor through a desiccant dryer system yielding at maximum 5000 SCFM of dry air at 125 psi a enabling continuous operation. The propane combustor is housed upstream of the nozzle section an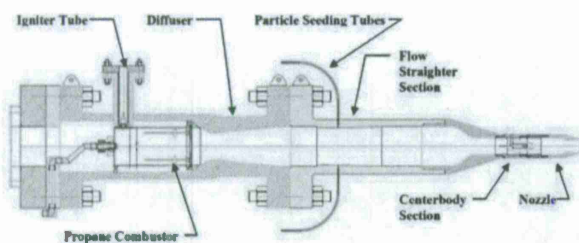d is followed by a ceramic flow conditioner and settling chamber upstream of the main contraction. Figure 3 shows the nozzle assembly which includes a centerbody housing and the nozzle section. When the centerbody was not used, a straight extension tube was put in its place so that the nozzle exit remained in the same location for all test configurations.

Figure 2 shows the AJL with all the data acquisition equipment in place during the experiment discussed herein. To date, PIV data was only acquired for one of the jet configurations under consideration. All of the acoustic data presented below were acquired in the second test entry for which the PIV camera and light sheet optics were removed from the room to have as anechoic an environment as possible.

Jet Nozzle Configurations

The jet nozzle assembly is modular offering the ability to test various inner-nozzle contours as shown in Fig. 4(a). The inner-contour inserts are locked in place with a threaded locking ring. This modularity also allows for a faceted inner contour to be generated by placing a number of identical segments inside the outer nozzle shell as shown in Fig. 4(b).

Three jet nozzle hardware configurations were considered during this work. They are referred to in the following discussion as the Baseline, Centerbody, and Faceted configurations according to the following descriptions.

Baseline The baseline configuration used the axisymmetric, conic, converging-diverging (C-D) nozzle. The term 'conic' is descriptive of the conic sections that make up the converging and diverging parts of the nozzle. These conic sections are brought together at a very sharp throat radius causing a near discontinuity in the wall slope at the throat. The baseline configuration did *not* include the centerbody section. The nozzle exit diameter $D_j = 2$ in., and the $AR = A_e/A_t = 1.4$.
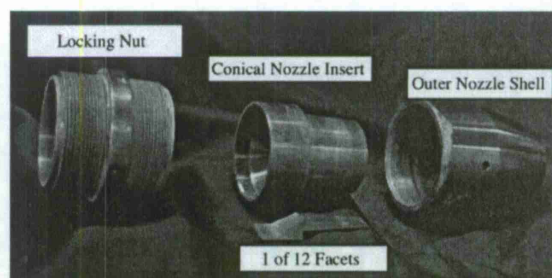
(a) Nozzle Parts

(b) Faceted Nozzle Assembly

FIGURE 4. The modular nozzle assembly allows for both axisymmetric and segmented inserts to be used for the inner-nozzle contour.

Centerbody The centerbody configuration used the conic nozzle but included a streamlined centerbody upstream of the nozzle contraction. The location of the centerbody is illustrated in both Fig. 1 and 3.

Faceted The faceted configuration utilized 12 identical segments to form the C-D nozzle contour as shown in Fig. 4(b). The exit-to-throat area ratio for the faceted nozzle is the same as that of the baseline conical nozzle. In the acoustic data for the Faceted configuration the centerbody was not used.

Jet Operating Conditions

Each of the three hardware configurations were operated at both over-expanded and fully-expanded M_j. The associated operating conditions are tabulated in Tab. 1. In all cases, the jet temperature was maintained at approximately 1005 K yielding a temperature ratio of 3.3. Table 1 also includes the $\beta^2 = M_j^2 - 1$ parameter which is known to be a significant parameter for broadband shock associated noise [10–12].

3

Copyright © 2012 by ASME

	NPR	M_j	T_j/T_a	β
Over-Expanded	3.92	1.55	3.3	1.18
Fully-Expanded	5.21	1.74	3.3	1.42

TABLE 1. Mean operating conditions for the over-expanded and fully-expanded jets.
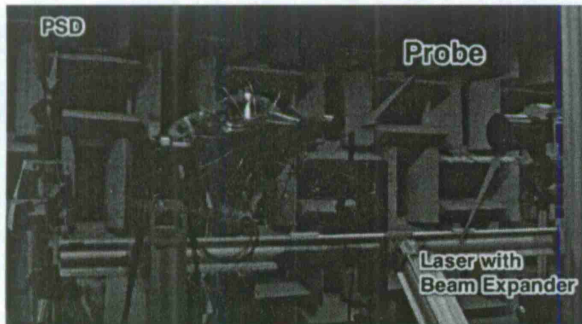

FIGURE 5. The pitot probe setup for the mean flow measurements included a 3-axis computer-controlled traversing system and a laser-based position sensitive detector (PSD) to correct axial position for the thermal expansion of the nozzle.

Mean Flow Profile Traversing System

A traversing total pressure (pitot) probe was used to characterize the mean jet flow for each configuration (see Fig. 5). The probe was positioned using a three-axis traverse system with greater than 0.1 mm accuracy. A centerline profile was measured after first determining the actual jet axis through a set of cross-stream profiles.Detailed cross-stream profiles were then measured at four distinct axial positions in order to characterize the mean flow evolution for each configuration.

Anticipating the difficulty in resolving the large gradients across shocks and the shear layers, an adaptive algorithm was developed to vary the step size taken by the traverse along the radial direction.By using this algorithm, without any foreknowledge of the mean flow, more points are taken in regions with larger total pressure gradients. This algorithm was implemented on the cross-stream profiles only.

For all total pressure measurements, the probe was traversed to the desired (x, r) position, allowed to settle, and then pressure measurements were acquired until the statistical 99% confidence interval fell below a specified 1% relative error. Once this confidence interval was achieved, the ensemble average was taken as the total pressure at that position. Each total pressure, $P_t(x, r)$ was subsequently normalized by the nozzle total pressure varia-

tion according to

$$P_t^*(x, r) = \frac{P_t(x, r)}{P_0} \cdot \overline{P_0} \qquad (1)$$

where P_0 is the ensemble mean of the jet stagnation pressure while the probe remained in one measurement station and $\overline{P_0}$ is the mean of all the ensemble means. This effectively removes any variation in the probe measurements caused by fluctuations in the jet stagnation pressure. Finally, the Rayleigh supersonic pitot formula was applied for measurements obtained within supersonic flow.

During long test runs, the thermal expansion of the nozzle assembly can be as much as 15% of the nozzle exit diameter. To account for this, the position of the nozzle exit was continuously tracked using an expanded He-Ne laser beam and a position-sensitive detector (PSD). The system was calibrated by traversing the nozzle itself through the beam, so that the PSD output voltage was recorded for a sequence of known positions. During each profile measurement, the PSD voltage was recorded at regular intervals.This data was used to correct the probe's axial position from the nozzle to within 1%.

Acoustic Arrays

Measurements of the near- and far-field pressures were acquired synchronously to develop an intuition for how changes to the jet flow structure would affect the far-field sound. Signatures registered in the hydrodynamic periphery of the jet produce a pressure footprint corresponding to the passage of large scale turbulent structures [13–16].

Near-Field Line Array A line array was constructed for near-field measurements and comprised thirty-one Kulite XT-140-100A transducers as shown in Fig. 6. These are absolute pressure transducers which have a range of 0-100 psia, a diameter of nominally 2.6 mm, and include a protective grid cap. Signal conditioning and amplification were provided by a National Instruments PXI system using an NI-PXIe-1073 chassis with an NI-TB-4330 board and four NI-PXIe-4331 cards (8 channels/card) with built-in anti-aliasing filters. All channels were sampled synchronously at 100kHz and phase aligned with the far-field measurements through an external trigger input.

The position of the near-field array relative to the jet axis is shown in Fig. 7. The most upstream microphone was located at $x/D_j = 1.6$ and $y/D_j = 1.87$, and the line array was set to an 8° angle relative to the jet axis. The spatial separation between adjacent points was chosen based on the integral scales of the flow. This was estimated from previous jet data [17] to be around 1/3 the shear layer thickness. The shear layer thickness is measured by the distance between the inner (4°) and outer (8°)
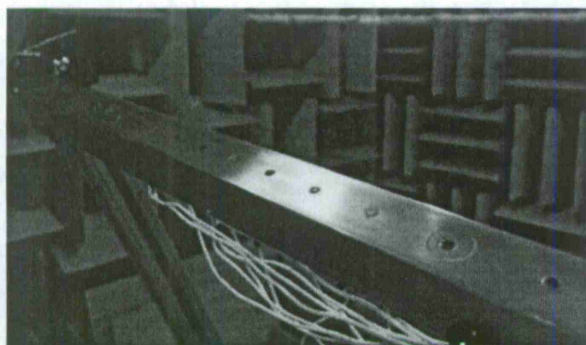
4

FIGURE 6. Photo of the upstream end of the near-field line array showing the small Kulite transducers flush-mounted in the aluminum housing.
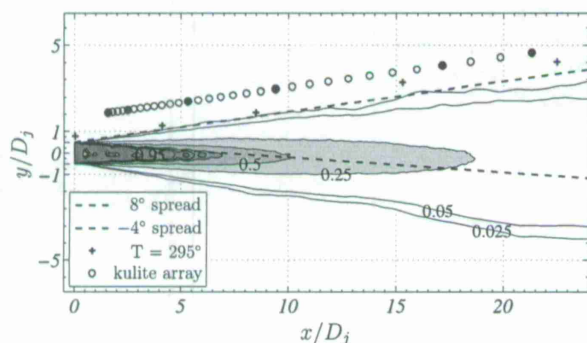

FIGURE 8. The position of the far-field arc array microphones relative to the nozzle exit.

FIGURE 7. Position of the near-field pressure array relative to a Mach 1.5 heated jet simulated by way of LES.

passage of turbulent large scale structures in the jet shear layer.

Far-Field Arc Array The far-field arc array consists of 12 B&K Type 4939 1/4-inch, free-field microphones attached to Type 2670 pre-amplifiers. The grid caps were removed during the experiments. Microphones were placed between 20° and 135° with closer spacing near the peak noise directions as shown in Fig. 8. Signal acquisition was performed using a National Instruments PXIe-4497 dynamic signal analyzer (16 simultaneously sampled analog input channels, 24 bit resolution) housed in a PXIe-1082 system. All channels were simultaneously sampled at 100 kHz and phase aligned with the near-field measurement through an external trigger input.

MHz Rate PIV System

The megahertz rate PIV system used in this work involved the combined use of a pulse burst laser (PBL) and a high-speed, gated intensified CCD framing camera. For its ability to acquire sequences of sixteen images at MHz rates, the system allowed time-resolved and high dynamic range measurements to be obtained for a heated, supersonic jet. Each component of the system is explained in detail below along with the experimental setup.

Pulse Burst Laser System As has been described in previous publications, [18–20] a PBL system developed at Auburn University allows a specified number of high-energy, MHz rate laser pulses to be formed from a given burst of low-energy, short-duration pulses. It should be noted that several upgrades have been made to this system since these publications: a new JDSU NPRO 126 continuous-wave (CW) Nd:YAG laser to enhance the pulse-to-pulse stability of each burst and three supplementary amplification stages (for a total of six amplification

spreading angles of the jet which were determined from preliminary LES computations performed by CRAFT Tech. In doing so, the length of the array could be designed to capture signatures registered between the near-nozzle region and the post-potential core region without compromising spatial resolution.

Tests conducted at UT-Austin compared the output of a Kulite to a standard 1/4-inch pressure field microphone (PCB) by placing both transducers within the hydrodynamic periphery of a perfectly expanded Mach 3.0 jet. Spectra computed from the Kulite revealed a steeper roll-off at the higher frequencies when compared to the 1/4-inch PCB microphone. This is caused by the small vent holes on the Kulite's protective grid cap which dampens out higher frequencies. Nevertheless, it was determined that this high-frequency roll-off was above the frequencies of interest in this case, and the Kulite transducers and 1/4-inch PCB microphones matched well at lower frequencies allowing successful measurement of the hydrodynamic hump corresponding to the
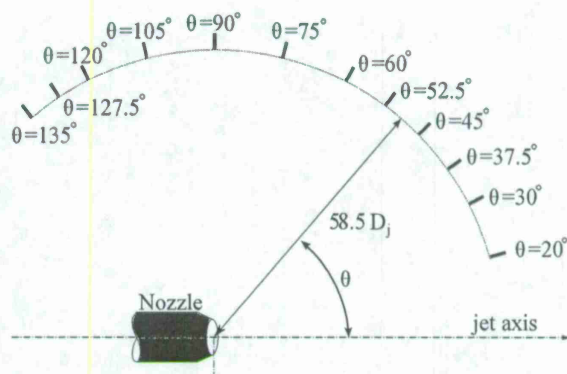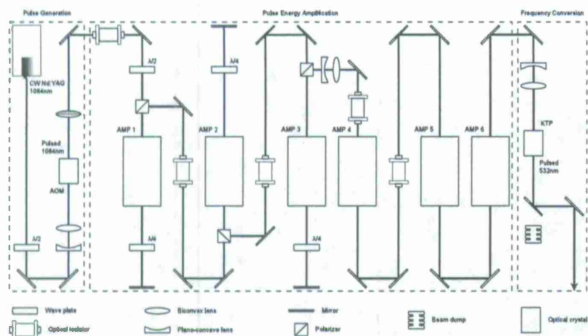
5

FIGURE 9. A top view of schematic of the pulse burst laser (PBL) system utilized for MHz rate PIV.

stages) to increase the overall energy available for each burst. A schematic of the upgraded PBL system is shown in Fig. 9.

The design of the PBL can be divided into three fundamental parts as indicated in the schematic: the pulse generation, the pulse energy amplification, and the frequency conversion. The pulse generation stage slices the output of the CW laser into a burst of low-energy, short-duration pulses through the use of an acousto-optic modulator (AOM) that relies on the principles of the acousto-optic (AO) effect. In particular, a piezoelectric transducer is used to produce acoustic waves inside an optical crystal such that the traveling waves cause variations in the index of refraction of the crystal. To an optical beam, these variations appear as a sinusoidal grating in which the wavelength is equal to the acoustic wavelength. By controlling when and how frequently acoustic waves are produced in the crystal, the generation of a specified number of short-duration pulses is possible depending on how often the CW input beam is disturbed. As with most AO devices, the AOM operates in the Bragg regime where most of the incident light can be diffracted into the first-order beam fairly efficiently. Here this diffracted beam constitutes the desired burst of pulses.

Following the formation of low-energy (nano-Joule order), short-duration pulses, the remaining stages of the pulse burst laser consist of pulse energy amplification and frequency conversion. Amplification is provided by six flashlamp-pumped Nd:YAG rod amplifiers of increasing diameter resulting in sufficient energy for fluid dynamic measurements. The first three amplifiers are used in a double-pass arrangement whereas the final three allow only for a single pass. Wave plates and polarizers provide the necessary means for achieving double-passes through the first three amplifiers. Optical isolators between each of the first five amplification stages prevent problems associated with parasitic lasing and amplified spontaneous emission (ASE). By the end of the amplification chain, pulse energies have increased by a factor of more than 10^7 and generally reach levels

in excess of 50 mJ/pulse[1].

The final stage of the PBL is the conversion of the beam's wavelength from 1064 nm to 532 nm. This conversion is achieved via a nonlinear process inside a KTP crystal and results in an unavoidable loss of pulse energy. Nevertheless, the beam, now in the visible spectrum, can be used for fluid dynamic measurements including PIV and flow visualization applications.

Cordin 222-4G High-Speed Camera Images were acquired using a Cordin 222-4G gated intensified CCD framing camera that is capable of recording sixteen images at a maximum, equally-spaced rate of 2,187,500 frames-per-second[2]. Image resolution is 2048×2048 pixels although the true resolution is slightly less due to the intensification process. The camera is able to achieve extremely high acquisition rates because it contains eight independently-controlled optical pathways, each incorporating a micro-channel plate (MCP) for signal intensification and ultimately terminating with a Kodak KAI-4022 CCD sensor. By allowing each CCD to record two images, sixteen total images can be acquired over a user-specified time period. Furthermore, because each pathway is independently operated, temporal spacing between frames is variable and can be set in an asynchronous fashion. Such flexibility even allows eight simultaneous exposures to be made. This feature is especially desirable since it enables eight nearly identical velocity fields to be obtained, with any differences being directly attributable to systematic error. For the experiments of interest, it is sufficient to note that because the camera can acquire sixteen images over a user-specified, extremely short time period, temporal-resolution is possible for all captured fluid motions. Additionally, the ability to obtain several particle images at varying time intervals relative to one another provides the means of performing high dynamic range PIV. Such measurements offer significant improvements over conventional PIV results since optimal time separations can be selected for different particle locations depending on the local velocity.

Setup of the MHz PIV System The MHz PIV system was only used to acquire data for the Baseline nozzle configuration at the over-expanded condition ($M_j = 1.55$). The field of view was centered at $x/D_j = 7$ and $r/D_j = -0.5$. This distance was chosen to coincide with the region around the end of the potential core. The region imaged was slightly less than 4 square inches and was illuminated by a laser sheet directed vertically upwards and spanning axially along the centerline of the jet. This

---

[1] This value is measured after the frequency conversion stage and thus accounts for the loss in energy associated with doubling the frequency of the Nd:YAG laser beam via a KTP crystal.

[2] This rate assumes a necessary CCD transfer time of 3.2 μs (specified by Cordin) to ensure that the second exposure does not include ghost images from the first exposure.
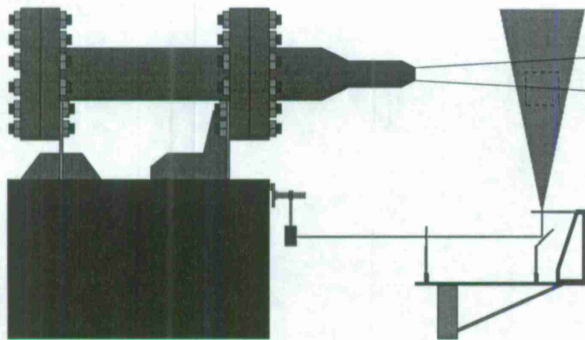
6

FIGURE 10. Experimental arrangement for the time-resolved, high dynamic range PIV application (side view). The square region enclosed by the dashed line indicates the camera's field of view.

FIGURE 11. Schematic of the synchronized data acquisition between the near-field and far-field microphone arrays and the MHz PIV system.

particular orientation was chosen for a variety of reasons, including both the need to minimize disruptions in the anechoic environment as well as to ensure the most direct observation of any shear layer without passing the light sheet through the jet prior to imaging. This last point was especially important to prevent problems associated with aero-optical distortions.

A schematic of the experimental setup is shown in Fig. 10. The 532 nm wavelength beam from the pulse burst laser was passed into the anechoic room perpendicularly to the jet axis and opposite the location of the camera. A turning mirror attached to the stand for the burner system allowed the beam to be directed downstream of the jet nozzle exit before encountering a 1000 mm biconvex spherical lens and a second turning mirror. The beam was then redirected vertically upwards through a cylindrical lens to form the laser sheet required for light scattering. Extreme care was taken to ensure that this light sheet was oriented both orthogonally to the axis of the camera lens as well as to the nozzle exit plane. Additionally, the placement of the spherical lens allowed the thinnest portion of the light sheet to persist across the camera's field of view.

Particle seeding of the jet was achieved using aluminum oxide (Al_2O_3) particles nominally 0.1 μm in size. A nitrogen-pressurized reservoir filled with these particles was connected to the burner system's particle seeding tubes shown in Fig. 3. Four seeding tubes were attached around the burner system symmetrically to provide a uniform seeding density throughout the jet.

PIV measurements were obtained by synchronizing the framing rate of the camera with the pulse generating rate of the pulse burst laser system. The chosen rate for all cases was 1 MHz, meaning the 16 images acquired by the camera enclosed a temporal window spanning 15 μs. To achieve the most consistent pulse-to-pulse intensity within each burst, 60 laser pulses were generated for a given burst, and the most stable 16 pulses were selected for synchronization with the 16 camera frames.
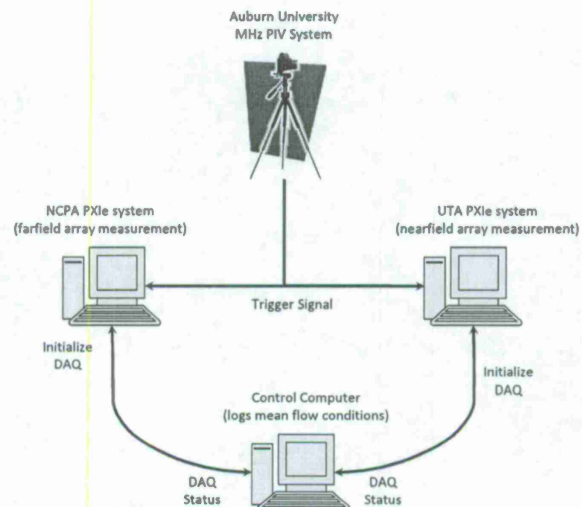
The duration of each laser pulse was approximately 20 ns such that no image streaking was observed. A Nikon Nikkor F-mount 70-300 mm objective zoom lens (f/4-5.6G) was used with the Cordin camera to acquire all image sequences.

Synchronizing the Data Acquisition Systems

The entire data acquisition system was purposely installed in such a way that time synchronization could be achieved across all three measurements: near-field pressure, far-field pressure, and PIV velocity. The goal of this arrangement is to allow for investigation of the flow-field events related to the generation of the measured jet noise.

The long transfer time needed to move each 16-image sequence from the camera to the PIV acquisition computer resulted in approximately 10 seconds between each 16-image acquisition. This being the slowest of the systems in terms of its data acquisition cycle (initialization, acquisition, saving) it was necessary utilize it as the trigger for the pressure acquisition systems.

Figure 11 shows a schematic view of the synchronized data acquisition process; this process was implemented using Lab-VIEW virtual instrument programs utilizing Data Socket communication and hardware TTL triggers for initiation.

The procedure for obtaining the synchronized data involved (a) bringing the jet up to predetermined set-point conditions of pressure and temperature and holding these conditions continuously, (b) the control computer initializing the near-field and far-field PXIe systems setting data acquisition parameters and generating a consistent filename on each system, (c) setting the

7

Copyright © 2012 by ASME

pressure acquisition systems in a reference trigger mode wherein they wait for a TTL trigger to start acquiring data, (d) sending the TTL trigger from the Cordin camera to the PXI units to initiate an acquisition cycle. The system operates in a continuous mode such that on each trigger signal from the camera both PXIe systems acquire and save dynamic data on their respective computers. The status of each PXIe system during data acquisition is communicated to the control computer which is also recording and averaging run conditions during the test event.

PRELIMINARY RESULTS FROM MHZ PIV
High Dynamic Range PIV

The ability to obtain several particle images at varying time intervals with respect to one another provides the means of performing high dynamic range PIV (HDR-PIV). For such measurements the dynamic velocity range is determined by the maximum and minimum resolvable particle displacements. Unlike conventional PIV where only one temporal spacing is available for all velocity determinations, the various combinations of image pairs in HDR-PIV enable velocity measurements to be made by utilizing optimal time separations for different regions of a flow field depending on the local velocity. Thus in regions of a flow field where little or no motion is observed between consecutive images, a larger temporal spacing (i.e., a pair of images separated by a greater time displacement) can be used such that the particle motions approach the optimal value for accurate cross-correlation analyses. This method offers substantial improvements over conventional PIV measurements and is especially useful in flows containing a wide velocity range. [21]

A schematic illustrating the capabilities of the HDR-PIV system is shown in Fig. 12. As mentioned, sequences of 16 images were obtained in which the time displacement, δt, between subsequent frames was 1 μs. For this arrangement the velocity field temporally located between frames 8 and 9 can be measured using different combinations of the 8 image pairs symmetrically straddling this t_0 point. It should be noted that other velocity fields could also be calculated; however this particular point in time allows the maximum number of image pairs to be used with the more accurate central finite-difference scheme. For regions of the velocity field containing the highest local velocities (i.e., the largest particle displacements between consecutive images), the image pair shown in red can be used to obtain the velocity. Likewise for regions containing little or no particle motions, an image pair spanning a larger temporal distance can be chosen. The image pair shown in blue represents the case of maximum time displacement and spans the entire sequence window of 15 δt or 15 μs. By using the information available across all 16 frames instead of only consecutive images, significant improvements in mean flow measurements as well as turbulence quantities can be made. This procedure will be utilized in the near future to analyze the collected data.
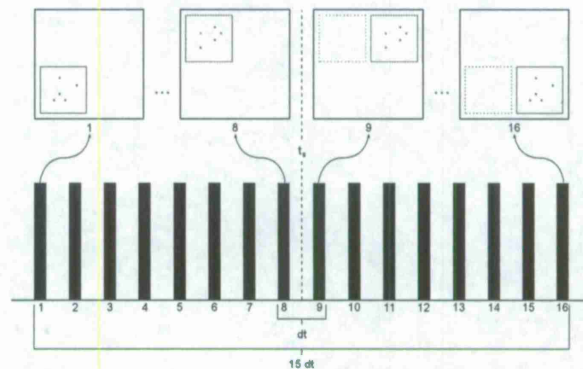

FIGURE 12. Illustration showing the basic principle of HDR-PIV. A single velocity field at t_0 can be determined by combining local velocity measurements acquired from various image pairs. Depending on the local velocity, image pairs are chosen such that optimal particle displacements occur between them.
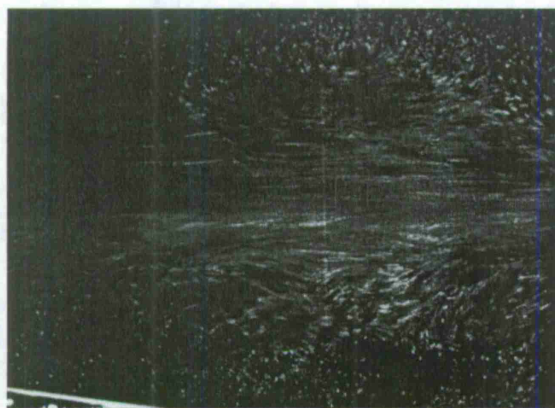
Pulse Burst Laser Flow Visualization

To illustrate the general characteristics of the flow field, a 60-pulse burst from the PBL was imaged using a PCO.Edge sCMOS camera. The image shown in Fig. 13 was recorded for the Centerbody configuration at $M_j = 1.55$. The center of the image is located near $x/D_j = 7$. Distinct vortical structures of relatively large size can be clearly identified in the shear layer.

Using the PBL for flow visualization causes the high-speed particles to appear in the image as dotted streaks. In regions of the flow where the individual dots can be resolved, it is possible to determine the direction, velocity, and acceleration along the streak. As an example of a potential image processing method, Fig. 13(b) shows a single 128-by-128 pixel interrogation area extracted from near the centerline of the jet (represented by a square in Fig. 13(a). A simple auto-correlation of the sample region reveals multiple peaks as shown in Fig. 13(c). The angle of the dotted line in the auto-correlation gives direction. The spacing between dots in the auto-correlation gives velocity magnitude when taken together with the time between pulses. Also, if a change in the distance between dots were evident, it may be possible to measure acceleration. However, due to the high velocity gradients, the particle streaks in the low-speed portion of the flow appear as solid and not dotted. This further illustrates the potential benefits of the HDR-PIV analysis.
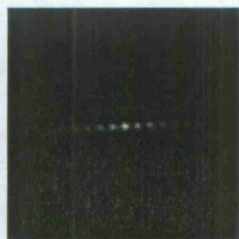
FLOW FIELD CHARACTERISTICS
Mean Flow Profiles

The centerline profiles for each nozzle configuration are shown in Fig. 14. The position of each point has been corrected for nozzle thermal expansion by a third-order polynomial fit to

8

(a) 60-Pulse Burst Imaged with a PCO.Edge Camera
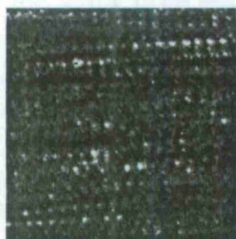
(b) 128-Pixel Sample   (c) Sample Auto-Correlation

FIGURE 13. PBL flow visualization of the $M_j = 1.55$ Centerbody configuration. The full image (a) is centered near $x/D_j = 7$.

FIGURE 14. Profiles of the total pressure decay along the get centerline. The end of the potential core is denoted by $\triangledown$, and the end of the supersonic core is denoted by $\square$.

the calibrated positions based on the PSD data. The error implicit in this method is estimated by the root of the residual sum of squares to be less than 0.03 jet diameters in all cases, except for that of the faceted nozzle where unexplained PSD voltage fluctuations yield a 0.5 jet diameter error. The shock cell structure is evident in all the centerline total-pressure profiles up to near the end of the potential core. For each case, the end of the potential core is denoted by a $\triangledown$, and the end of the supersonic core is denoted by a $\square$. It is significant that the supersonic core extends downstream approximately 2 times the length of the potential core. And, even though the mean profile suggests the influence of shocks stops at the end of the potential core, the hydrodynamic pressure field illustrated in Fig. 18 clearly shows that the shock related oscillations have an effect up to the end of the supersonic core. Therefore, shocks of weakening strength are likely present throughout the supersonic region but may be masked by turbulent fluctuations in these mean pressure measurements.

The mean, cross-stream, total pressure profiles for the Baseline and Centerbody configurations for both $M_j = 1.74$ and $M_j = 1.55$ are shown in Fig. 15. In the mean, there was no observed difference between the Baseline and Faceted cases, so the
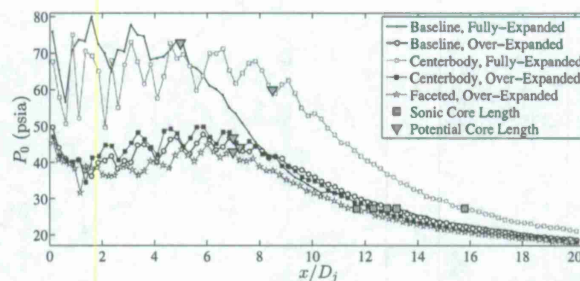
Faceted data is not shown. The x/D_j position of each profile is shown above each profile and has been corrected for nozzle expansion as discussed above. The evolution of the jet profile shape from a near top-hat to a self-similar hyperbolic sine function is evident as is the effect of the probe traversing across shocks in the near-nozzle profiles. The centerbody itself is supported by three streamlined pylons equally spaced azimuthally around the annulus inside the enclosing pipe. The wake from one of these pylons was in the profile plane and is the cause for the observed asymmetry in the Centerbody configuration.

Far-Field Acoustic Characteristics
The single-sided auto-spectral density (SPL) of the far-field pressure signals were generated using an ensemble average of 150 sets of 4096 samples yielding a frequency resolution of $\Delta_f = 24.4$ Hz. The spectra are shown in Fig. 16 for both the over-expanded ($M_j = 1.55$) and fully-expanded ($M_j = 1.74$) jet conditions. Beginning with the downstream observer at $\theta = 20°$, subsequent spectra are shifted by 15 dB for clarity.

As expected, far-field jet noise is dominated by turbulent mixing noise at shallow angles. And, at the over-expanded M_j (Fig. 16(a)) broadband shock noise (BBSN) in the steeper angles is more dominant compared to the fully-expanded M_j. Furthermore, below the Mach wave angle of this jet – where sound pressure levels form to create the classic heart-shape pattern of jet noise – the nozzle configuration has little influence on the spectral levels. However, between the Mach wave angle and the steeper angles, the effects introduced by the centerbody or faceted inner contour are evident and shown to reside in the high frequency band. This suggests that the predominant effect of inclusion of a centerbody or a faceted nozzle contour will be noticed in the higher frequencies and in the steeper angles.

The observed directivity of the measured overall sound pressure level (OASPL) for each nozzle configuration is shown in Fig. 17 for both the over-expanded and fully-expanded M_j. There is an interesting difference between the Baseline and Faceted
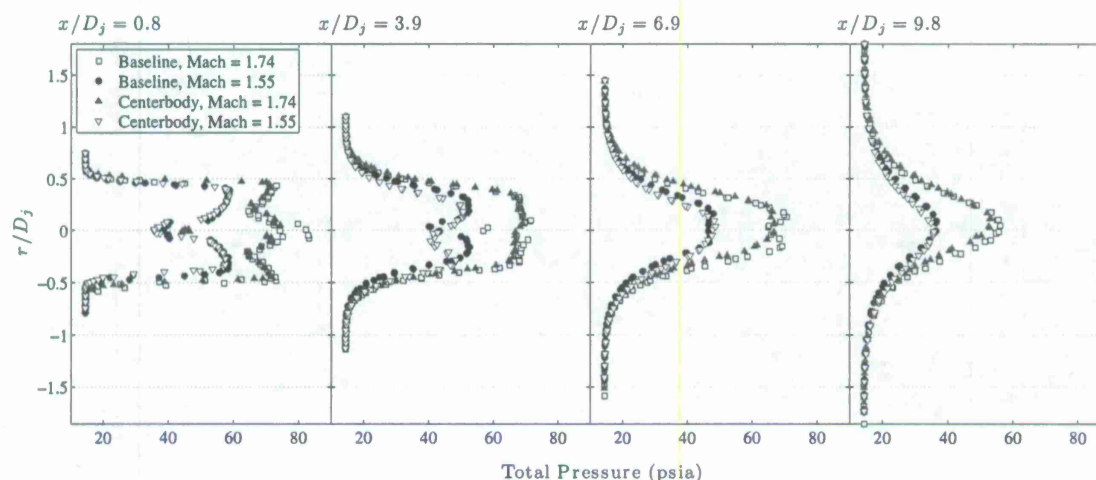
9   Copyright © 2012 by ASME

FIGURE 15. r/D_j profiles of the total pressure, P_t, for the Baseline and Centerbody configurations. The axial x/D_j is shown directly above each profile.

cases, particularly in the upstream, shock-noise dominated direction. At the over-expanded M_j, the OASPL near 120° is higher for the Faceted nozzle while at the fully-expanded M_j the opposite is true. This suggests that the faceted inner contour is significant in the organization of the shocks.

The Mach wave angles calculated for the over-expanded and fully-expanded operating conditions are 47.3° and 52.8°, respectively. This is based on the convective Mach number of the jet. Baars *et al.* [22] has shown this value to range from $0.6M_a$ for heated jets to $0.8M_a$ for cold jets. The acoustic Mach number (M_a) is the ratio between the jet exit velocity (U_j) and the ambient sound speed ($\sqrt{\gamma_a R_a T_a}$). A convective Mach number of $0.6M_a$ is found in the current study and can be confirmed with the space-time contours in Fig. 18. Figure 17 supports these values in that the maximum overall sound pressure level for the fully-expanded condition occurs at a steeper angle than that of the over-expanded condition, indicating that Mach waves propagate from a location several diameters downstream of the jet exit.

Near-Field Acoustic Characteristics

An illustration of the raw time series acquired with the near-field array is shown in Fig. 18 for the baseline nozzle. The presence of shock cells in the jet plume is evident in the periodic nature of the contours in the figure. These shock cells are present even when the nozzle is operated at $M_j = M_d$ (fully-expanded) due to internal shock that forms because of the non-ideal inner-nozzle contour. These signatures are very different than those found in perfectly expanded (shock-free) flows [22, 23]. The effect of the shock cells on the near-field pressure is evident out

to as far as fifteen diameters downstream from the nozzle exit. For the baseline contour the supersonic core is estimated to end around $x/D_j = 13$; the potential core collapses around $x/D_j = 7$ and 5 for the over-expanded and fully-expanded conditions, respectively. This suggests that the region between the end of the potential core and the end of the supersonic core may be of significance for the aeroacoustics of supersonic, shock-containing jets.

Overall sound pressure levels (OASPL) are shown in Fig. 19. The region between the collapse of the potential core and the end of the supersonic core contains the most intense turbulence activity and is thought to be the location responsible for the most intense sound production. Variations in the upstream flow conditions are shown in Fig. 19(a) and 19(b) to have little to no effect on the OASPL. In Fig. 19(c), the fully-expanded nozzle is shown to comprise a greater abundance of energy than the over-expanded nozzle, as would be expected due to the higher exit velocity.

Single-sided power spectral densities (SPL) of the near-field pressure are shown in Fig. 20 for the over-expanded ($M_j = 1.55$) and fully-expanded ($M_j = 1.74$) jet conditions. These spectra were generated using an ensemble average of 150 sets of 4096 samples yielding a frequency resolution of $\Delta_f = 24.4$ Hz. In each figure, six Kulites have been selected to provide a general overview of the signatures registered in this region of the flow and the effects caused by upstream flow conditions (center-body and faceted). Subsequent spectra are shifted by 20 dB. The influence of the internal flow conditions are shown to have a lasting effect on the lower band of frequencies (below the hydrodynamic ridge) due to a thicker boundary layer or higher turbulence lev-
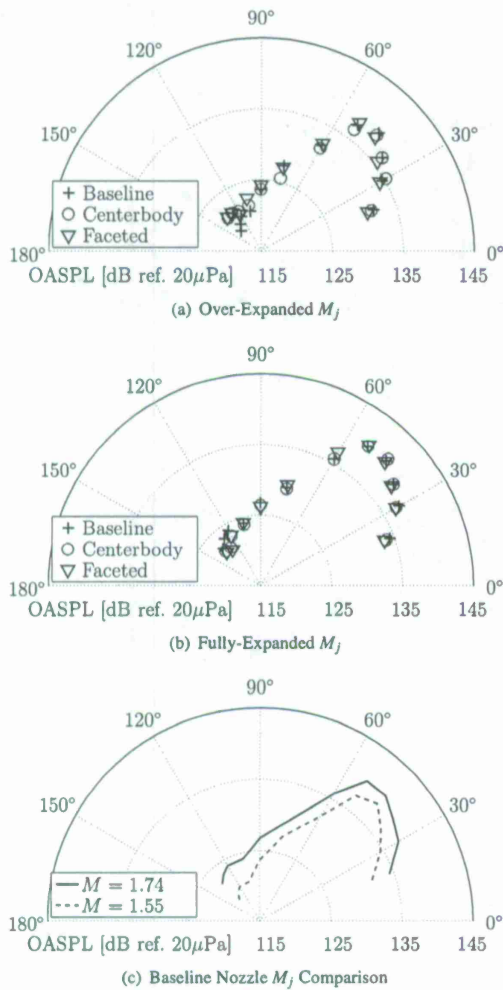
10

(a) Over-Expanded M_j

(b) Fully-Expanded M_j

(c) Baseline Nozzle M_j Comparison

FIGURE 17. Overall sound pressure level (OASPL) from the far-field array. Comparison of inflow conditions for the (a) over-expanded and (b) fully-expanded nozzles. (c) Comparison of OASPL between over- and fully-expanded base inflow condition.

els at the nozzle exit. In particular, the centerbody produces a low-frequency pulsation that is more pronounced for the over-expanded flow. Periodically shedding vortices that form in the wake of the centerbody are believed to be responsible for this. Surprisingly, this wake appears to have little influence on the hydrodynamic ridge formed by the jet column mode. Likewise, the evanescent signatures produced by these shedding events appear not to be affected by the jet shear layer as they emanate a recognizable signature several jet diameters downstream.
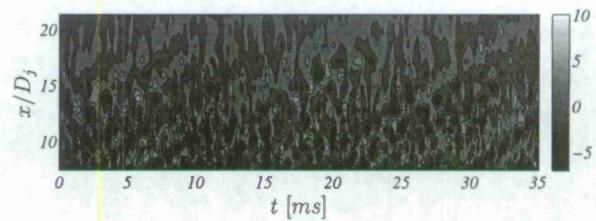

FIGURE 18. Space-time contours of the raw fluctuating pressure along the near-field array (in 10^3 Pa).

(a) Over-Expanded M_j

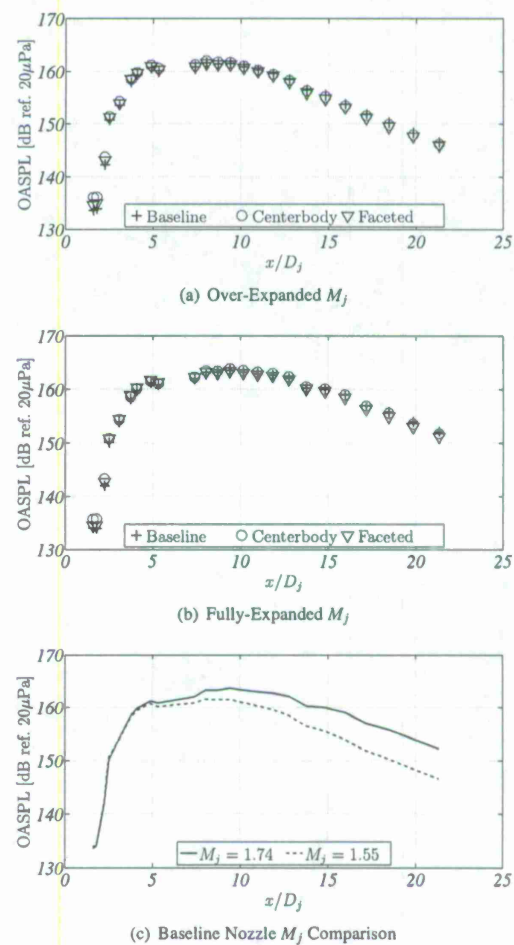(b) Fully-Expanded M_j

(c) Baseline Nozzle M_j Comparison

FIGURE 19. Overall sound pressure level (OASPL) from the near-field array. Comparison of inflow conditions for the (a) over-expanded and (b) fully-expanded nozzles. (c) Comparison of OASPL between over- and fully-expanded base inflow condition.
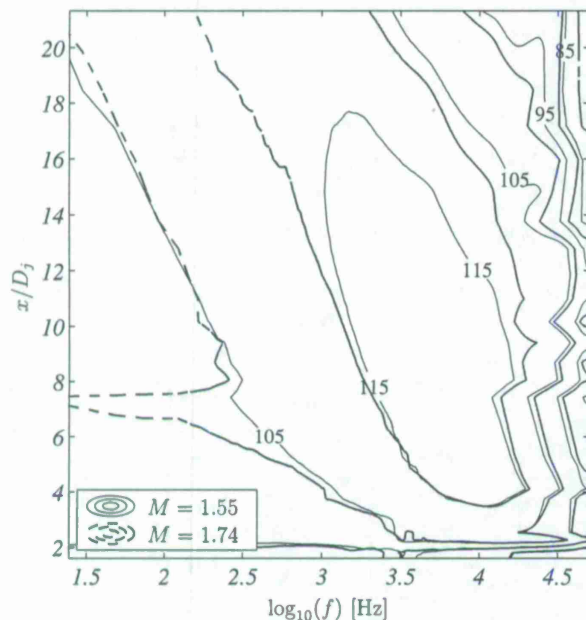
11

FIGURE 21. Comparison of SPL [dB/Hz] contours for the base nozzle configuration.

Because of the existence of shocks near the nozzle exit, several tones are expected. These tones are more easily captured by a near-field observer. The tones in the range of several kilohertz are eventually masked by the broader energy from turbulent mixing toward the downstream locations. These findings are consistent with existing studies of jet noise [24] and include characteristic turbulent mixing noise, broadband shock associated noise, and tones associated with screech.

In an effort to compare the baseline conditions between the over-expanded and fully-expanded nozzles, contours of the SPL are shown in Fig. 21. The frequency axis has been plotted using a base-10 logarithmic scale to reveal the nearly perfect logarithmic decay in the peak frequency with increasing distance downstream (increasing shear layer growth). Following the work of Ewing *et al.* [25], it has been recently shown by Tinney & Jordan [26] how the characteristic axial wavenumbers of the near-field pressure are homogeneous in this region and that a collapse of the two-point correlation, obtained between two fixed points, can be written with a function that depends only on variables obtained from a self similar solution. A logarithmic similarity coordinate of the form $\ln(x') - \ln(x)$ worked very well for the near-field study of Tinney & Jordan (see [25] for details concerning this similarity solution) and would appear to work equally as well for both base flow conditions here, given the logarithmic shift in the spectral peak with increasing distance shown in Fig. 21.

OBSERVATIONS

There are three primary observations of note based on the data presented herein. First, the flow visualization clearly identifies coherent structures of significant size near the end of the potential core region. Second, the far-field acoustics suggests that the effect of the inclusion of a centerbody or a faceted nozzle contour is predominately observed in the higher frequencies and the steeper angles. Finally, the near-field pressure measurements indicate that the influence of the shocks in the jet extend all the way to the end of the supersonic core in the jet plume – suggesting the region between the end of the potential core and the end of the supersonic core may be of significance for the aeroacoustics of supersonic, shock-containing jets.

FUTURE WORK

Future work will focus on the completion of the HDR-PIV analysis. It is planned that the synchronous data acquisition system will be employed to acquire data for each nozzle configuration. The resulting high-fidelity PIV data will be utilized to examine the 2-point correlations both within the jet and between the jet and the near-field and far-field pressure. As additional focus will be to determine the roll of the supersonic core length in the observed jet noise.

ACKNOWLEGDEMENTS

REFERENCES

[1] Munday, D., Gutmark, E., Liu, J., and Kailasanath, K., 2011. "Flow structure and acoustics of supersonic jets from conical convergent-divergent nozzles". *Physics of Fluids*, *23*, p. 116102.

[2] Kuo, C.-W., Veltin, J., and Mclaughlin, D. K., 2009. "Acoustic measurements of models of military style supersonic nozzle jets". In 47th AIAA Aerospace Sciences Meeting, no. 2009-0018.

[3] Bridges, J., 2006. "Effect of heat on space-time correlations in jets". In 12th AIAA Aeroacoustics Conference, no. 2006-2534.

[4] Wernet, M., 2007. "Time resolved piv for space-time correlations in hot jets". In 45th AIAA Aerospace Sciences Meeting and Exhibit, no. 2006-0047, AIAA.

[5] Seiner, J., and Yu, J., 1984. "Acoustic near-field properties associated with broadband shock noise". *AIAA Journal*, *22*(9), pp. 1207–1215.

[6] Doty, M., and McLaughlin, D., 2002. "Two-point correlations of density gradient fluctuations in high speed jets

12   Copyright © 2012 by ASME

using optical deflectometry". In 40th AIAA Aerospace Sciences Meeting, no. 2002-0367.

[7] Papamoschou, D., Morris, P., and McLaughlin, D., 2010. "Beamformed flow-acoustic correlations in a supersonic jet". *AIAA Journal,* *48*(10), pp. 2445–2453.

[8] Ponton, M., Seiner, J., Ukeiley, L., and Jansen, B., 2001. "A new anechoic chamber design for testing high-temperature jet flows". In 7th AIAA/CEAS Aeroacoustics Conference and Exhibit, no. 2001-2190, AIAA.

[9] Ukeiley, L., Tinney, C., Mann, R., and Glauser, M., 2007. "Spatial correlations in a transonic jet". *AIAA Journal,* *45*(6), pp. 1357–1369.

[10] Harper-Bourne, M., and Fisher, M. J., 1974. The noise from shock waves in supersonic jets. Tech. Rep. CP 131, 11.1-11.13, AGARD.

[11] Norum, T., and Seiner, J., 1982. "Broadband shock noise from supersonic jets". *AIAA Journal,* *20*(1), pp. 68–73.

[12] Pao, S., and Seiner, J., 1983. "Shock-associated noise in supersonic jets". *AIAA Journal,* *21*(5), pp. 687–693.

[13] Arndt, R., Long, D., and Glauser, M., 1997. "The proper orthogonal decomposition of pressure fluctuations surrounding a turbulent jet". *Journal of Fluid Mechanics,* *340*, pp. 1–33.

[14] Lau, J. C., Fisher, M. J., and Fuchs, H. V., 1972. "The intrinsic structure of turbulent jets". *Journal of Sound and Vibration,* *22*, pp. 379–406.

[15] Picard, C., and Delville, J., 2000. "Pressure velocity couping in a subsonic round jet". *International Journal of Heat and Fluid Flow,* *21*, pp. 359–364.

[16] Tinney, C. E., Ukeiley, L. S., and Glauser, M. N., 2008. "Low-dimensional characteristics of a transonic jet. part 2: Estimate and far-field prediction". *Journal of Fluid Mechanics,* *615*, pp. 53–92.

[17] Tinney, C. E., Glauser, M. N., and Ukeiley, L. S., 2008. "Low-dimensional characteristics of a transonic jet. part 1: Proper orthogonal decomposition". *Journal of Fluid Mechanics,* *612*, pp. 107–141.

[18] Lempert, W., Wu, P., Zhang, B., Miles, R., Lowrance, J., Mastracola, V., and Kosonocky, W. "Pulseburst laser system for high speed flow diagnostics". *AIAA Paper*, No. 96-0179, 1996.

[19] Wernet, M., and Opalski, A. "Development and application of a mhz frame rate digital particle image velocimetry system". *AIAA Paper*, No. 2004-2184, 2004.

[20] Thurow, B., Satija, A., and Lynch, K., 2009. "Third-generation megahertz-rate pulse burst laser system". *Applied Optics,* *48*(11), pp. 2086–2093.

[21] Hain, R., and Kähler, C., 2007. "Fundamentals of multi-frame particle image velocimetry (piv)". *Experiments in Fluids,* *42*(4), pp. 575–587.

[22] Baars, W. J., Tinney, C. E., Murray, N. E., Jansen, B. J., and Panickar, P., 2011. "The effect of heat on turbulent

mixing noise in supersonic jets". In 49th AIAA Aerospace Sciences Meeting including the New Horizons Forum and Aerospace Exposition, no. 2011-1029, AIAA.

[23] Baars, W. J., Tinney, C. E., and Wochner, M. S., 2012. "Nonlinear noise propagation from a fully expanded mach 3 jet". In 50th AIAA Aerospace Science Meeting, no. 2012-1177.

[24] Tam, C., 1995. "Supersonic jet noise". *Annual Review of Fluid Mechanics,* *27*, pp. 17–43.

[25] Ewing, D., Frohnapfel, B., George, W. K., Pedersen, J. M., and Westerweel, J., 2007. "Two-point similarity in the round jet". *Journal of Fluid Mechanics,* *557*, pp. 309–330.

[26] Tinney, C. E., and Jordan, P., 2008. "The near pressure field of co-axial subsonic jets". *Journal of Fluid Mechanics,* *611*, pp. 175–204.
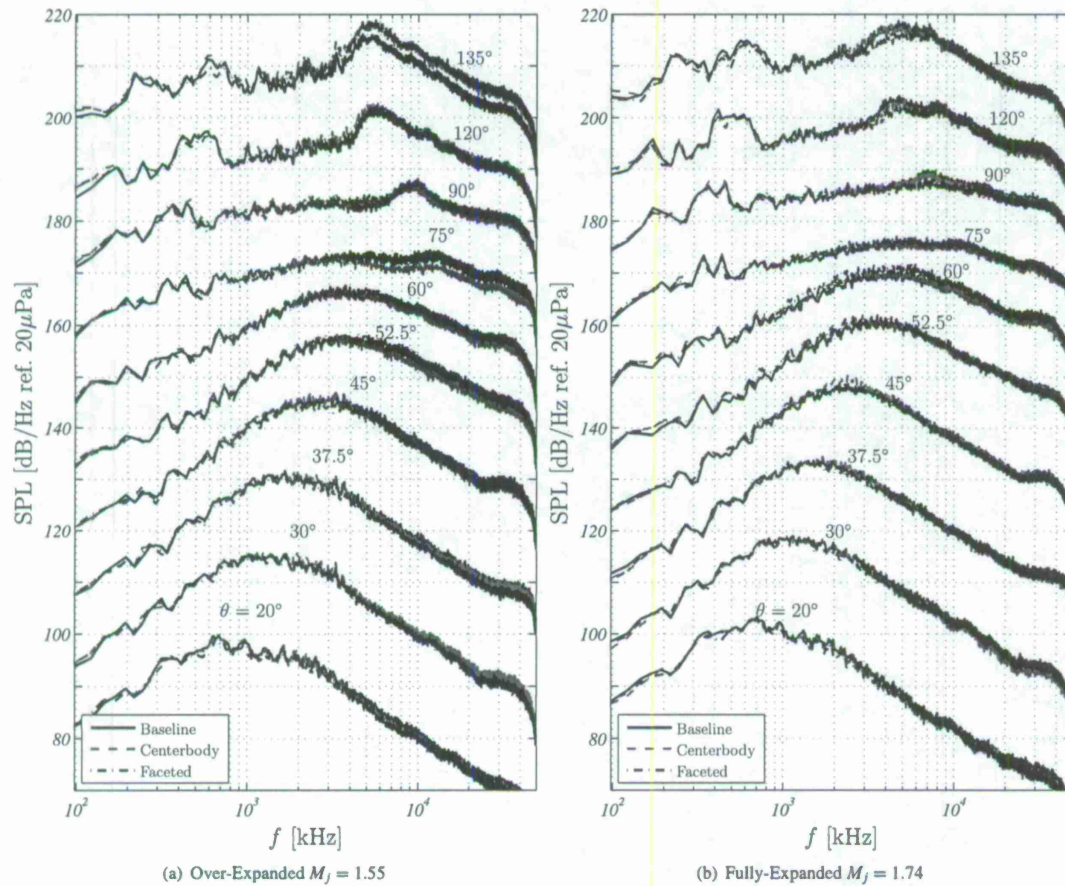
13

(a) Over-Expanded $M_J = 1.55$

(b) Fully-Expanded $M_J = 1.74$

FIGURE 16. Single-sided power spectral densities (SPL) of the far-field pressure. SPLs are shifted cumulatively by 15 dB.

14

(a) Over-Expanded $M_j = 1.55$ (b) Fully-Expanded $M_j = 1.74$
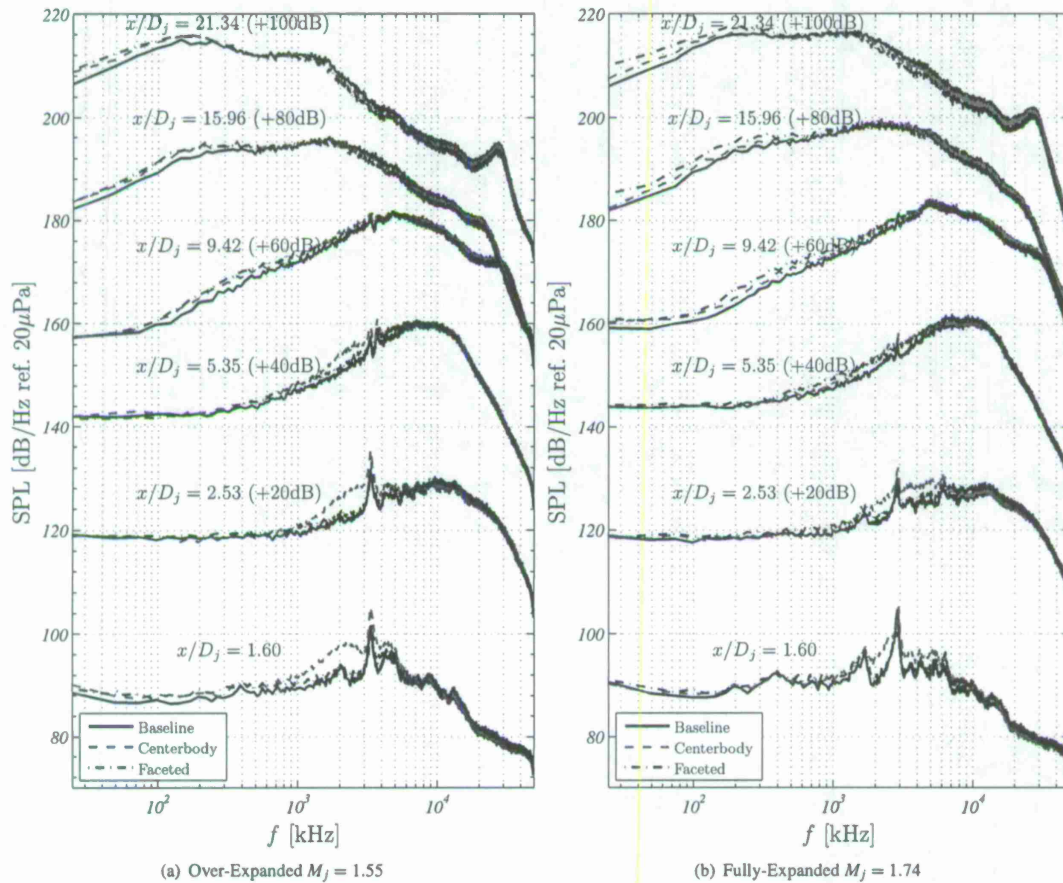
FIGURE 20. Single-sided power spectral densities (SPL) of the near-field pressure from the over expanded nozzle (Mach 1.55). SPLs are shifted cumulatively by 20 dB.

15